Received: 17 August 2023 | Revised: 7 April 2024 | Accepted: 3 May 2024

DOI: 10.1002/qj.4782

Quarterly Journal of the Royal Meteorological Society RMetS

RESEARCH ARTICLE

A momentum budget study of the semi-annual oscillation in the Whole Atmosphere Community Climate Model

Aleena M. Jaison[1] | **Lesley J. Gray**[1,2] | **Scott Osprey**[1,2] | **Anne K. Smith**[3] | **Rolando R. Garcia**[3]

[1]Atmospheric, Oceanic and Planetary Physics, University of Oxford, Oxford, UK

[2]National Centre for Atmospheric Science, Oxford, UK

[3]Atmospheric Chemistry Observations and Modeling, National Center for Atmospheric Research, Boulder, Colorado, USA

Correspondence
Aleena M. Jaison, Atmospheric, Oceanic and Planetary Physics, University of Oxford, Oxford, UK.
Email: aleena.moolakkunneljaison@physics.ox.ac.uk

Abstract

The representation of the semi-annual oscillation (SAO) in climate models shows a common easterly bias of several tens of metres per second compared to observations. These biases could be due to deficiencies in eastward tropical wave forcing, the position or strength of the climatological summertime jet or the strength/timing of the Brewer–Dobson circulation. This motivates further analysis of the momentum budget of the upper stratosphere within models and a more detailed comparison with reanalyses to determine the origin of the bias. In this study, the transformed Eulerian mean momentum equation is used to evaluate the different forcing terms that contribute to the SAO in the MERRA2 reanalysis dataset. This is then compared with the equivalent analysis using data from a climate simulation of the Whole Atmosphere Community Climate Model (WACCM). The comparison shows that WACCM underestimates eastward forcing by both resolved and parameterised waves at equatorial latitudes when compared with MERRA2 and also has a weaker tropical upwelling above 1 hPa.

KEYWORDS

Brewer–Dobson circulation, equatorial waves, quasi-biennial oscillation, semi-annual oscillation, stratosphere

1 | INTRODUCTION

The stratospheric semi-annual oscillation (SAO) is characterised by oscillating wind and temperature fields with a periodicity of six months in the equatorial upper stratosphere and lower mesosphere. The SAO dominates equatorial variability between 0.3 and 5 hPa, in the region above the quasi-biennial oscillation (QBO). It has been suggested that both oscillations influence surface weather through various pathways, including their influence on the winter polar vortex (Anstey et al., 2022; Baldwin et al., 2001; Gray et al., 2020). The first documentation of the SAO was based on rocket sonde observations in the tropics by Reed (1966). Even though there are still some uncertainties among observations and reanalyses (SPARC, 2022 Chapter 11), substantial progress has been made in understanding the mechanisms of the SAO since then.

The zonal wind SAO near the stratopause consists of easterly phases that occur around the solstices, December–February (DJF) and June–August (JJA), and

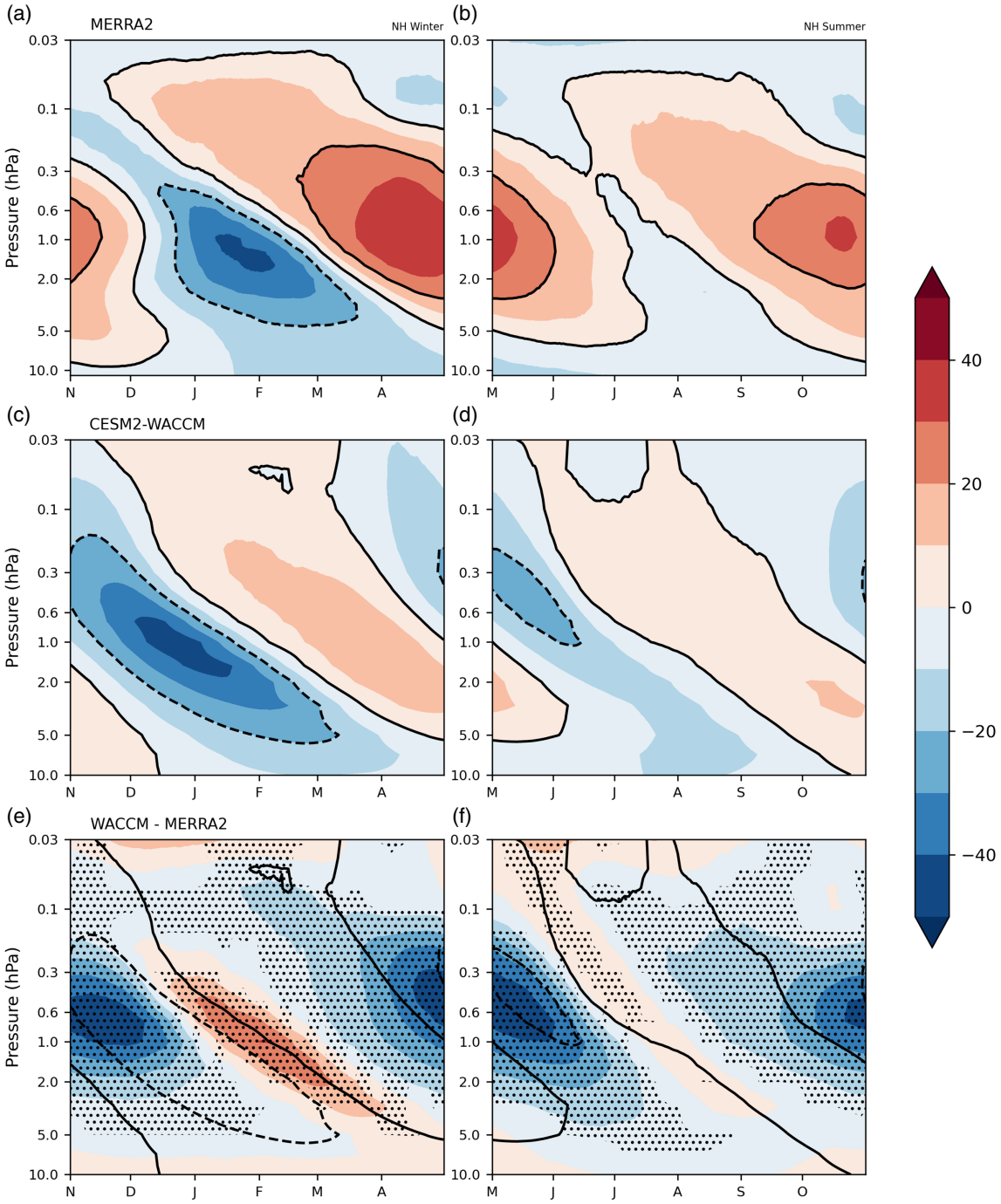

FIGURE 1 Daily mean climatology of zonal-mean zonal wind ($m \cdot s^{-1}$) averaged over 5° N to 5° S for (a,b) Modern-Era Retrospective Analysis for Research and Applications, Version 2 (MERRA 2) based on 42 years (1980–2021). (c,d) Whole Atmosphere community climate model (WACCM), based on the first 500 years of the CMIP6 pi-Control simulation (see Section 2 for details). Contours of −20, 0, 20 $m \cdot s^{-1}$ are overlaid, with dashed contours denoting negative values. For clarity, the time axis has been separated and centred around the onset of the easterly phase. (e,f) WACCM minus MERRA2 differences, with overlaid wind contours from the WACCM distribution. Stippling denotes 99% confidence interval.

westerly phases around the equinoxes, March–May (MAM) and September–November (SON) (Hirota, 1980; Reed, 1966). Figure 1a,b shows the climatological equatorial zonal-mean zonal winds from the Modern-Era Retrospective Analysis for Research and Applications, Version 2 (MERRA2) reanalysis dataset. The time series are shown in six-month sub-sections (November–April and May–October), centred around the MERRA2 peaks in stratopause easterlies that occur in February and August. In this way, we can highlight the differences between the

first and second SAO cycles that contribute to the presence of an annual cycle.

The magnitudes of the peak easterlies and westerlies are similar, at around 30–40 $m \cdot s^{-1}$, but the easterly phase centred around Northern Hemisphere (NH) winter is stronger than the summer phase, so there is also an annual component to the equatorial stratopause variability (Delisi & Dunkerton, 1988; Quiroz & Miller, 1967). The semi-annual nature of the zonal wind variability is clearly visible within ~10 degrees north and south of the equator. At higher latitudes annual harmonics dominate (Ray et al., 1998). The SAO easterly phase onset occurs almost simultaneously at heights between 0.5 and 5 hPa while the westerly phase starts at a higher altitude and gradually descends over time (Quiroz & Miller, 1967). The underlying QBO is also known to modulate the SAO (Smith et al., 2023). The SAO westerly phases (SAOW) are observed to be stronger during the easterly phase of the QBO (QBOE) and, as the QBOE descends, the successive SAOW phases also extend farther down in altitude. Once in every four to six SAO cycles the SAOW propagates sufficiently far down to merge with the onset of the westerly phase of the QBO (Dunkerton & Delisi, 1997; Garcia et al., 1997; Gray & Pyle, 1989; Krismer et al., 2013). Garcia et al. (1997) presented a comprehensive study of the SAO climatology in the tropical stratosphere using multiple observations, which has since been updated using reanalysis datasets and more recent observations (Smith et al., 2017; Kawatani et al., 2020; SPARC, 2022, Chapter 11). Ern et al. (2021) recently examined the SAO and the gravity wave (GW) forcing using these observational datasets.

The semi-annual nature of the oscillation was first explained using radiative forcing ideas, as the sun crosses the equator twice a year (Webb, 1967). However, it was noted that radiative forcing cannot drive tropical oscillations (Wallace, 1967; Wallace & Holton, 1968) and wave forcing was suggested as a major driver (Meyer, 1970). Extensive research since then has indicated that the westerly phase of the SAO is driven primarily by vertically propagating tropical waves, although this is difficult to explicitly confirm due to the lack of high-resolution observations at SAO altitudes. Planetary-scale Kelvin waves and inertia-GWs (Garcia, 2000; Hirota, 1978) as well as small scale eastward-propagating GWs (Ern et al., 2021; Hamilton & Mahlman, 1988; Hitchman & Leovy, 1986, 1988) are all believed to contribute to the SAO westerly forcing. While relatively slow eastward-propagating waves are absorbed at lower levels in the westerly QBO region, high-speed waves can propagate through to the SAO region where they are damped and transfer their momentum to the background flow (Dunkerton, 1979; Hirota, 1978). The observed weaker SAO westerlies during the westerly phase of QBO can thus be explained since the waves are more likely to be absorbed in the lower stratosphere during a westerly QBO phase than during the easterly QBO phase.

The simultaneous onset of the easterly phase of the stratospheric SAO over a range of altitudes suggests that it is likely associated with the meridional circulation (Holton & Wehrbein, 1980). Two sources of westward momentum have been proposed for the easterly SAO phase. Firstly, the meridional cross-equatorial advection of easterlies from the summer to winter hemisphere by the residual mean meridional circulation, which is primarily driven by eddy forcing in the extratropical, winter stratosphere (Holton & Wehrbein, 1980). The weaker easterly SAO phase in the second half of the year can then be explained, since there is less planetary wave forcing at midlatitudes in the Southern Hemisphere (SH) winter, and thus a weaker residual mean meridional circulation. Secondly, the lateral momentum transfer by more localised quasi-stationary waves in the winter hemisphere subtropics has been suggested as an additional westward momentum source (Hopkins, 1975). Affirming this, Ern et al. (2015) have highlighted a strong westward forcing by planetary-scale waves at the onset of SAO easterly jets using ERA-Interim reanalysis data.

We note that while the eastward forcing is associated with vertically propagating wave absorption, the westward forcing is associated with meridional advection and extratropical eddy forcing which peak during the winter of each hemisphere, so it is this westward forcing that gives rise to the semi-annual nature of the oscillation. This contrasts with the QBO, in which both phases are primarily due to wave forcing.

Inertial instability is another important phenomenon that is present in the middle atmosphere, caused by the imbalance of the horizontal pressure gradient and the Coriolis force; several studies have explored the relevance of this mechanism to the SAO (e.g., Hitchman & Leovy, 1986). Due to the advection of summer easterlies into the winter hemisphere, it has been noted that there is an increased possibility for inertial instabilities to develop in regions close to the equator, primarily within 0–10° latitude in the winter hemisphere, although they can also be found at higher latitudes due to flow distortions by Rossby waves (Rapp et al., 2018; Strube et al., 2020). Inertial instabilities at the equator result in an eastward forcing and thus the weakening of the SAO easterly phase (Dunkerton, 1981; Ray et al., 1998). Supporting this view, a recent case study by Lieberman et al. (2021) showed that during NH summer inertial instability sharply weakens the equatorial easterlies at the stratopause.

The SAO can impact atmospheric circulations in various ways. It can influence the distribution of chemical

tracers in the equatorial stratosphere, thus explaining a 'double peak' structure seen in upper stratospheric measurements of ozone and many other trace gases (Gray & Pyle, 1986; Shu et al., 2013). It has also been suggested to influence surface weather, in a similar manner to the well-studied QBO influence. The QBO is known to modulate both the extratropical circulation (Anstey & Shepherd, 2014; Holton & Tan, 1980) and also the subtropical circulation through the locally induced meridional circulation required to maintain thermal wind balance (Garfinkel & Hartmann, 2011; Gray et al., 2018), both of which may influence surface weather (Ebdon, 1975; Gray et al., 2018; Kidston et al., 2015; Marshall & Scaife, 2009). While the peak amplitude of the zonal-mean zonal wind SAO is observed to extend to ±10° latitude, its influence also extends poleward into the subtropical upper stratosphere via an induced meridional circulation. Model studies have suggested that the strength of subtropical upper stratospheric winds in early winter have an impact on the later evolution of the polar vortex; for example, whether it remains cold and undisturbed throughout the winter or whether it is disrupted by wave disturbances, with the possibility of a sudden stratospheric warming (SSW). In particular, Gray et al. (2004, 2022) found that wind anomalies in the subtropical upper stratosphere influence the timing of SSWs, with an easterly anomaly promoting an early to mid-winter SSW and a westerly bias promoting either a late-winter SSW or no SSW at all. This suggests that a good representation of the SAO may improve model simulations of the polar vortex evolution and SSW frequency. It is widely acknowledged that SSWs can affect surface weather and thus a good representation of their behaviour and frequency will be useful for improved weather prediction (Butler et al., 2016; Lu et al., 2021; Mukougawa et al., 2009; Scaife et al., 2005).

Climate model representation of the SAO has been examined by, for example, Smith et al. (2019) and has also been used to study aspects of the forcings responsible for the westerly and easterly phase of SAO (e.g., Ray et al., 1998). An easterly bias of the SAO in climate models is a long-standing problem; all climate models unambiguously show an easterly bias, although there are variations in the extent to which the SAO amplitude and altitude range differ (Smith et al., 2017; Smith et al., 2019). A case study by Müller et al. (1997) using the Berlin troposphere-stratosphere-mesosphere general circulation model and the model study of Smith et al. (2019) both suggest that insufficient Kelvin wave dissipation in the upper stratosphere could be a reason for the easterly bias, while Smith et al. (2019) also mention the possibility of differences in GW drag (GWD). However, none of these earlier studies have examined all of the individual driving mechanisms in order to draw a solid conclusion on the reason for the easterly bias.

The main aim of this paper is to understand the source of the easterly bias in the representation of the SAO in climate models. We do this by carefully examining individual contributions to the momentum budget of the SAO region in a specific climate model and comparing it with reanalyses, to determine which momentum-forcing terms are most influential and which terms contribute to the easterly bias. The paper is laid out as follows: Section 2 describes the data and analyses used in this study. Results are presented in Section 3 and Section 4 summarises our findings.

2 | DATA AND METHODS

This study utilises the transformed Eulerian mean momentum (TEM) equation to quantify the contribution of different momentum-forcing terms in both reanalysis and model. Comparisons between model and reanalysis terms are conducted to identify possible model biases. Three reanalysis datasets are initially evaluated: MERRA2, ERA-Interim and ERA5, which are described in Section 2.1. Based on this evaluation, the MERRA2 dataset is employed as the primary reanalysis dataset. CESM2-WACCM, described in Section 2.2, has been selected as the sample climate model for a more comprehensive investigation. It is a coupled chemistry model that extends much higher in altitude than most other models, which helps to avoid potential complications arising from having the model top close to SAO altitudes. It also demonstrates a reliable representation of the QBO, reducing the likelihood of QBO biases impacting the SAO. The methodology employed in the study, including the momentum budget analysis and estimation of statistical significance of our results, is described in Section 2.3.

2.1 | Reanalysis datasets

Three reanalysis datasets are examined: the Modern-Era Retrospective Analysis for Research and Applications, Version 2 (MERRA2), and the ERA-Interim and ERA5 reanalyses from the European Centre for Medium-Range Weather Forecasts (ECMWF).

MERRA2 (Gelaro et al., 2017) is a global reanalysis dataset provided by the National Aeronautics and Space Administration (NASA) Goddard Institute for Space Studies (GISS). The dataset used in this study extends over a 42-year period 1980–2021. It has a horizontal resolution of 0.5° latitude × 0.625° longitude and a vertical resolution of 72 hybrid-η model levels extending from the surface to 0.01 hPa. The Goddard Earth Observing System-5 (GEOS-5) model used to generate

the MERRA2 dataset includes parameterisations of both orographic (McFarlane, 1987) and non-orographic GW schemes (Garcia & Boville, 1994; Molod et al., 2015). The non-orographic GW scheme is optimised to enhance the representation of QBO and SAO in the tropics (Molod et al., 2015). Artificial damping (Rayleigh friction) is applied to horizontal winds at altitudes above 0.24 hPa. In addition to assimilating a large suite of ground-based and satellite observations (see SPARC, 2022 for a summary), MERRA2 has the added benefit of assimilating Microwave Limb Sounder (MLS) temperature observations at altitudes above 5 hPa after August 2004. The dataset is thus constrained by additional observations in the region of interest to this study.

ERA-interim (Dee et al., 2011) has a spectral horizontal resolution of T255 (∼79 km spacing on a reduced Gaussian grid) and vertical resolution of 60 model levels extending up to 0.1 hPa. The reanalysis is produced using ECMWF's Integrated Forecast System (IFS) cycle 31r2. The model includes an orographic GW parameterisation (Lott & Miller, 1997) but does not include a non-orographic GW parameterisation. Artificial damping (Rayleigh friction) of horizontal winds is employed at altitudes above 10 hPa.

ERA5 (Hersbach et al., 2020) employs IFS cycle 41r2, with horizontal and vertical resolution of T639 and 137 model levels, respectively. The highest altitude is at 0.01 hPa, similar to MERRA2. It additionally includes a non-orographic GW parameterisation scheme (Orr et al., 2010). A fourth-order hyper-diffusion (∇^4) is applied on vorticity, divergence and temperature above 10 hPa to damp vertically propagating waves depending on model level and zonal wavenumber and an additional first-order damping (∇) is applied on divergence above 1 hPa (Polichtchouk et al., 2017). In contrast to MERRA2, data from the MLS are not assimilated in ERA5 (SPARC, 2022).

2.2 | Model

CESM2-WACCM is the Community Earth System Model Version 2 (CESM2) Whole Atmosphere Community Climate Model (WACCM), which is the 'high-top' version of the coupled climate Earth system model developed by the National Center for Atmospheric Research (NCAR). The model includes a representation of both ocean and atmosphere with comprehensive component schemes for land, sea-ice, land-ice and river processes, interactive coupled atmospheric chemistry and ocean wave models that are linked via a coupler (Danabasoglu et al., 2020). The model has a horizontal resolution of approximately 1° (0.9° latitude × 1.25° longitude) and has 70 levels in the vertical from the surface to 6×10^{-6} hPa (approx.140 km). It thus has a superior stratospheric representation compared to the standard 'low top' version of CESM2-CAM (Danabasoglu et al., 2020). CESM2-WACCM (hereafter referred to as WACCM) includes orographic and non-orographic GWD parameterisation schemes (Richter et al., 2010), with orographic, frontal and convective GW sources separately specified, hence linking GW generation to tropospheric quantities to produce model-consistent GW source fluxes (Gettelman et al., 2019). The GW scheme provides wave forcing that contributes to the internally generated QBO and SAO. Further description of the model and other parameterisations can be found in Gettelman et al. (2019).

The model dataset used is the CMIP6 pre-industrial control (pi-Control) simulation (Eyring et al., 2016) from WACCM. This coupled atmosphere–ocean simulation was run with prescribed pre-industrial (1850) levels of greenhouse gas and aerosols. It therefore has no time-varying external forcing apart from daily and seasonal radiative variations, so any variability on other time scales is internally generated. We choose to use the WACCM pi-Control simulation, even though its imposed external forcings are not directly comparable with the MERRA2 reanalysis datasets, because the climatology of its forcing can be assessed with many more available years and its SAO climatology was found to be very similar to the corresponding WACCM present-day CMIP6 simulation. The CMIP6 data are published by the Earth System Grid Federation; more details on the WACCM pi-Control simulation can be found at Danabasoglu et al. (2019). All analyses were performed using data from the first 500 years of the simulation. For the power spectral analysis described in Section 3, only the first 42 years of data are used so that the data length matches that of MERRA2. Tests were performed to check that similar results were found with different 42-year intervals.

2.3 | Methodology

The zonal-mean momentum budget of the SAO is analysed using the TEM momentum equation (Andrews et al., 1987) in spherical geometry and log-pressure coordinates. This equation is obtained following a transformation of the zonally averaged Eulerian-mean fields in the primitive equations to better separate the relative contributions of advection and momentum fluxes to the evolution of zonal-mean zonal flow. The resulting equation is.

$$\frac{\partial \overline{u}}{\partial t} = -\overline{v}^* \left[\frac{1}{a\cos\phi} \frac{\partial \overline{u}\cos\phi}{\partial \phi} - f \right] - \overline{w}^* \frac{\partial \overline{u}}{\partial z} + \frac{1}{\rho_0 a \cos\phi} \nabla \cdot F + \overline{X}, \quad (1)$$

where

$$\overline{v}^* = \overline{v} - \frac{1}{\rho_0}\left(\frac{\rho_0\overline{v'\theta'}}{\overline{\theta}_z}\right)_z,$$

$$\overline{w}^* = \overline{w} + \frac{1}{a\cos\phi}\left(\frac{\cos\phi\overline{v'\theta'}}{\overline{\theta}_z}\right)_\phi,$$

$$\nabla\cdot F = \frac{1}{a\cos\phi}\frac{\partial}{\partial\phi}\left(F^{(\phi)}\cos\phi\right) + \frac{\partial F^{(z)}}{\partial z},$$

and,

$$F^{(\phi)} = \rho_0 a\cos\phi\left(\overline{u}_z\frac{\overline{v'\theta'}}{\overline{\theta}_z} - \overline{u'v'}\right),$$

$$F^{(z)} = \rho_0 a\cos\phi\left(\left[f - \frac{1}{a\cos\phi}\frac{\partial\overline{u}\cos\phi}{\partial\phi}\right]\frac{\overline{v'\theta'}}{\overline{\theta}_z} - \overline{w'u'}\right).$$

Using the three-hourly averaged horizontal and vertical winds and temperature fields (u, v, w, T) from the reanalysis datasets, TEM diagnostics contributing to the SAO forcing are calculated in the pressure coordinates and transformed into standard log-pressure vertical coordinates to obtain the formulation of Andrews et al. (1987) shown above (see Gerber & Manzini, 2016 and their corrigendum). For WACCM, the CMIP6 data archive repository includes the pre-calculated TEM variables. Daily mean values of the TEM variables are presented in this study.

The first two terms on the right-hand side of Equation (1) represent advection of zonal momentum due to the residual meridional and vertical velocities. This is associated in part with the residual meridional overturning circulation in the stratosphere, generally known as the Brewer–Dobson circulation (BDC), which involves upwelling in the summer hemisphere tropics, cross-equatorial flow with meridional movement through the winter midlatitudes and downwelling at high latitudes. Since the BDC in the mid-upper stratosphere is strongest at solstice and always flows from the summer to the winter hemisphere, the horizontal advection at those levels will be strongest at solstice (i.e., DJF and JJA) and will advect easterly momentum across the equator. The vertical advection contribution will depend on the strength of the Brewer–Dobson equatorial upwelling, the strength of any induced (secondary) circulation due to local wave activity, and the vertical gradient of the zonal wind.

The last two terms in Equation (1) represent the zonal-mean acceleration due to wave driving. The first of these is proportional to the divergence of the Eliassen–Palm (EP) Flux and arises from the dissipation of resolved waves, that is, those with large enough horizontal extent and temporal duration to be explicitly resolved in the model. A negative EP flux divergence generally implies the presence of westward-propagating waves such as planetary-scale Rossby waves, which transfer easterly momentum to the zonal flow, while a positive EP flux divergence is associated with the presence of eastward waves, such as Kelvin waves, which transfer westerly momentum. The term X includes the parameterised GW driving together with other residual forcing such as that due to numerical diffusion.

To assess statistical significance in model–reanalysis comparisons, a two-sided Student's t-test is used. The null-hypothesis states that the reanalysis and model data are drawn from the same underlying distribution and have identical statistical characteristics. A p-value less than 1% is considered indicative of a significant difference between the model and reanalysis means.

3 | RESULTS

3.1 | The SAO in reanalyses

Figure 2a–c shows the time–height section of equatorial daily-mean zonal-mean zonal winds (5° N–5° S) from the MERRA2, ERA-I and ERA5 reanalysis datasets for a sample of 10 years. Alternating westerlies and easterlies, consistent with the stratospheric SAO, are evident over an altitude range of 10–0.1 hPa.

While the three reanalysis datasets agree well in terms of the broad structure of the alternating winds that form the SAO, there are major differences, particularly in the strength and duration of the westerly phase. MERRA2 and ERA5 have stronger and longer-lasting westerly wind regimes, while ERA-I shows westerly and easterly phases that are similar in both strength and duration. The relatively weak SAOW in ERA-I is likely associated with the lack of a non-orographic GW parameterisation. However, the ERA5 reanalysis has unrealistically strong SAO westerlies (>70 mm·s^{-1}) near the stratopause, as noted by previous studies (Ern et al., 2021; Shepherd et al., 2018). The MERRA2 dataset is considered to be the more realistic when compared with Sounding of the Atmosphere using Broadband Emission Radiometry (SABER) and MLS observational data (Kawatani et al., 2020). MERRA2 assimilates MLS temperature data above 5 hPa starting in August 2004, so a close resemblance to the observations is perhaps not surprising (Ern et al., 2021; SPARC, 2022 Chapter 11). Nevertheless, the sharp weakening of the MERRA2 SAO amplitude above 0.03 hPa is unrealistic compared to observations (Kawatani et al., 2020). Since among the three reanalyses MERRA2 most closely resembles the winds derived from satellite observations, we use MERRA2 for comparison with the WACCM in the remainder of the study. We compare diagnostics for altitudes below 0.03 hPa because the WACCM CMIP6 TEM dataset was only archived up to this level, focusing primarily on the region below 0.24 hPa (the level where artificial damping is introduced in the MERRA2 dataset) to learn more about the forcing contributing to the peak in SAO amplitude centred around 1 hPa.

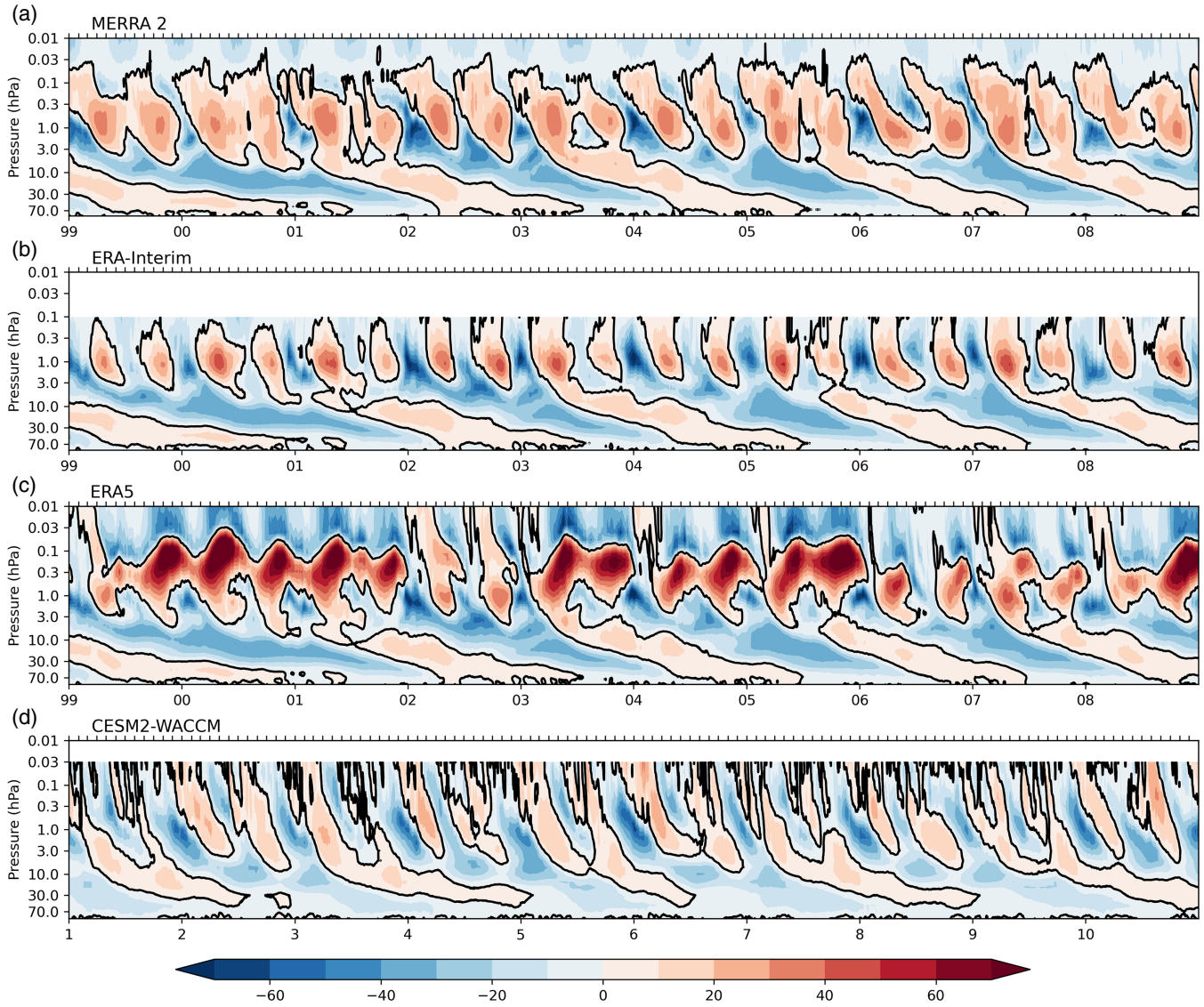

FIGURE 2 Zonal-mean zonal wind ($m \cdot s^{-1}$) averaged over 5° N to 5° S for the years 1999–2008 for (a) Modern-Era Retrospective Analysis for Research and Applications, Version 2 (MERRA 2), (b) ERA-interim, (c) ERA-5 and (d) a sample 10 years from the Whole Atmosphere Community Climate Model (WACCM) model simulation.

3.2 | The modelled SAO

The time–height section of daily-mean zonal-mean equatorial zonal winds (5° N–5° S) from WACCM for a sample of 10 years is shown in Figure 2d. The alternating westerlies and easterlies of the SAO over the altitude range of 10–0.1 hPa are similar to the reanalyses, including the gradual descent of the westerly phase so that it merges with the onset of the QBO westerly phase. However, the amplitudes of the easterly and westerly SAO phases are roughly equal in magnitude, similar to ERA-I, such that there is a noticeable easterly bias at ~1 hPa when compared with MERRA2.

The easterly bias is confirmed in Figure 3 which shows latitude–height sections of climatological zonal-mean zonal winds, averaged over each three-month seasonal window from MERRA2 (Figure 3a,d) and WACCM (Figure 3e–h), together with the WACCM minus MERRA2 difference (Figure 3i–l). A negative difference therefore denotes an easterly bias in WACCM, while a positive difference denotes a westerly bias. The most obvious differences between WACCM and MERRA2 in the SAO region are the weaker westerly regimes near 0.5 hPa at the equinoxes in WACCM. The model shows a maximum deviation from the reanalysis in the spring and autumn seasons, that is, during the SAOW. For example, during MAM and SON, MERRA2 has westerly winds extending from one hemisphere to the other with a secondary peak at equator. While the model captures this broad pattern, the equatorial westerlies are much weaker, by greater than 30 $m \cdot s^{-1}$ at the

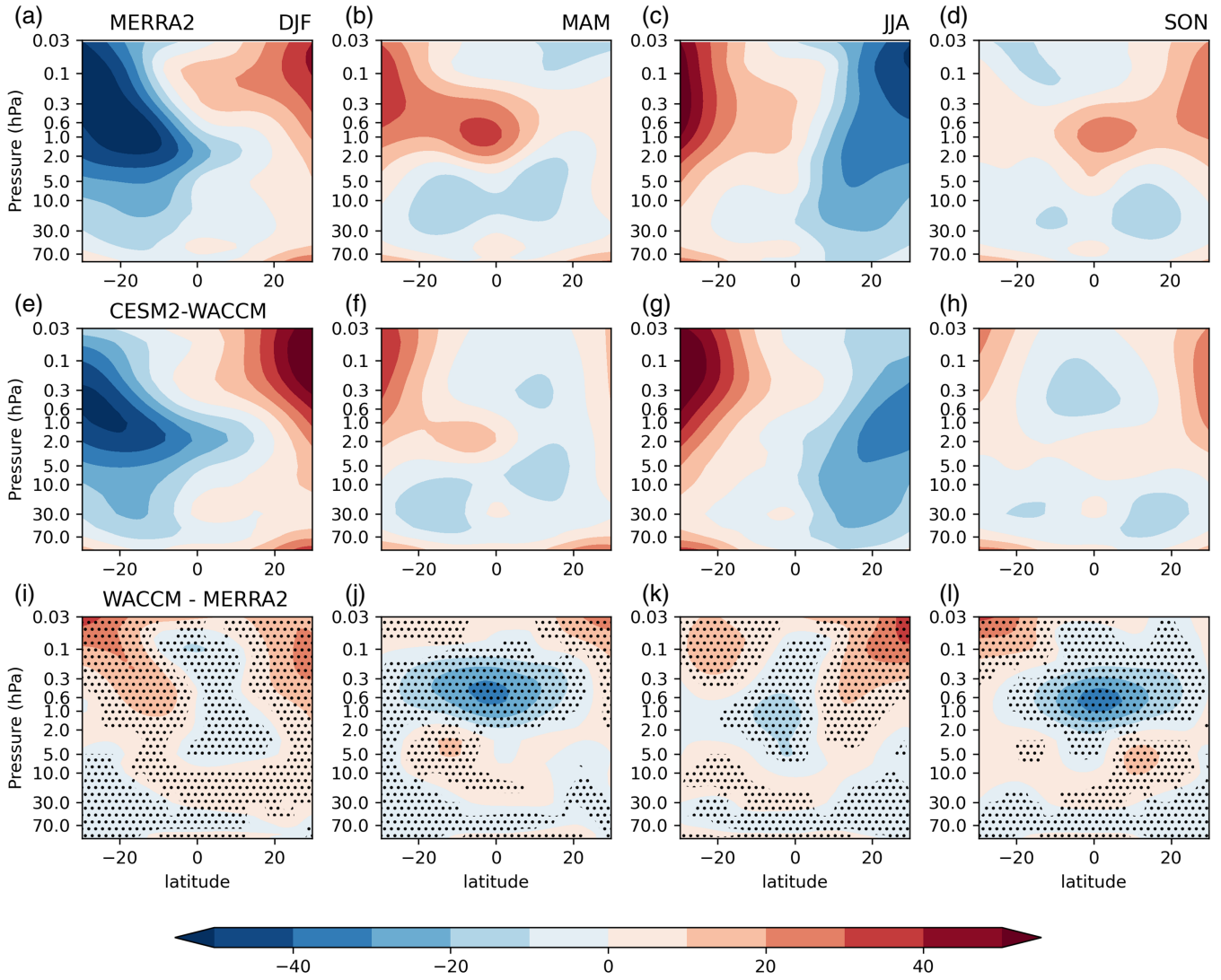

FIGURE 3 Latitude–height sections of three-month averaged zonal-mean zonal wind ($m \cdot s^{-1}$) between ±30 degrees latitude from (a–d) the Modern-Era Retrospective Analysis for Research and Applications, Version 2 (MERRA2) 42-year (1980–2021) climatology, (e–h) the 500-year Whole Atmosphere Community Climate Model (WACCM) climatology, and (i–l) the WACCM minus MERRA2 differences. Stippling denotes 99% confidence interval.

equinoxes (Figure 3j,l). The easterly phases in DJF and JJA are more comparable, although the 'nose' of easterlies that extends from the SH subtropics into equatorial latitudes at ~2 hPa in DJF is slightly overestimated in WACCM. The annual cycle is readily apparent at the equator in both MERRA2 and WACCM; for example, the DJF 1 hPa equatorial winds in MERRA2 and WACCM are $\sim -30\,m \cdot s^{-1}$ while in JJA, WACCM has easterlies of $-10\,m \cdot s^{-1}$ and MERRA2 still has westerlies.

To confirm the presence of the annual cycle, Figure 4 shows the frequency amplitude spectra of zonal-mean equatorial (5° S–5° N) zonal winds over a range of altitudes in the stratosphere, derived from the initial 42 years of WACCM data. It confirms that variability in both MERRA2 and WACCM is dominated by QBO periodicities of around two years at altitudes below 5 hPa, while between 5 and 0.1 hPa it is dominated by six-month SAO periodicities and a less pronounced annual variability, as noted above. However, the WACCM power is consistently lower across all frequencies, suggesting that the amplitudes of the QBO, SAO and annual variability are all underestimated in this 70-level version of WACCM. Note also that the WACCM QBO has a shorter period which shows up as a dipole in the differences plot.

3.3 | Momentum budget

In this section the primary focus is to examine the climatology of the different forcing terms that contribute to

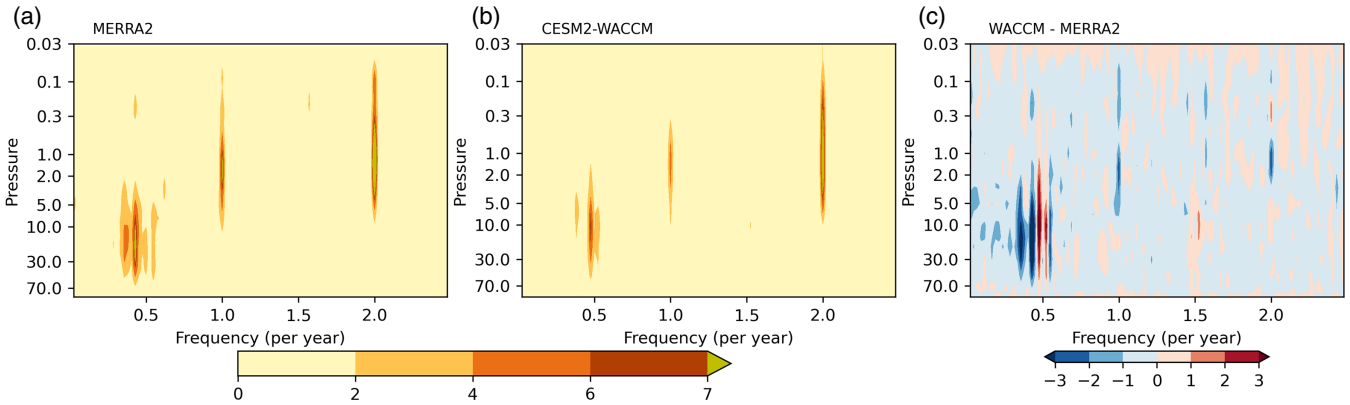

FIGURE 4 Frequency amplitude spectrum of climatological zonal-mean zonal wind from 5° S to 5° N as a function of altitude from (a) Modern-Era Retrospective Analysis for Research and Applications, Version 2 (MERRA2), (b) Whole Atmosphere Community Climate Model (WACCM) and (c) the WACCM minus MERRA2 differences. The colour contours are Fourier amplitudes (square root of power). Units are $m \cdot s^{-1}$.

the wind distributions in the SAO region. Returning to a closer examination of the zonal wind evolution shown in Figure 1, the peak winds of the westerly phase of the WACCM SAO (Figure 1c,d) are less than 20 $m \cdot s^{-1}$ for the majority of the period, while MERRA2 (Figure 1a,b) shows winds of up to 40 $m \cdot s^{-1}$. The onset of the WACCM easterly phase is too early; for example, at 1 hPa the WACCM westerlies reverse to easterlies in mid-April and October, almost two months before MERRA2. The onset of the WACCM westerly phase also occurs slightly early, compared to MERRA2, but the amplitude of the westerly phase fails to develop sufficiently strongly and does not last long enough compared to MERRA2. In summary, Figure 1 confirms the results of earlier studies (Smith et al., 2019) that WACCM, along with most other models, has a substantial easterly bias near the stratopause (see the difference plot [Figure 1e,f]). It also highlights a mismatch in the timing of the phase onsets.

To further investigate those factors influencing the SAO evolution, we examine the individual components of the TEM momentum equation, Equation (1), as described in Section 2. Figure 5 shows the time evolution of the climatological total rate of change of equatorial zonal-mean zonal winds from MERRA2 and WACCM averaged over ±5° latitude. The data are plotted only in the stratosphere above 10 hPa, such that the region dominated by the SAO is highlighted. Also plotted (in contours) are the respective climatological equatorial zonal winds from Figure 1.

In MERRA2 (Figure 5a,b) the strongest eastward acceleration is evident at the onset of both SAOWs, as expected, and follows the zero-wind contour as it descends with time. Similarly, the maximum westward acceleration is evident around the onset of each easterly phase. However, at the onset of the first easterly phase in November–January the maximum acceleration occurs simultaneously over a range of altitudes between 5 and 0.3 hPa, while it descends more gradually with time at the onset of the second easterly phase, starting at 0.3 hPa in May and descending to around 5 hPa by July.

For WACCM (Figure 5c,d), the corresponding time series shows similar behaviour, but with differences in timing that reflect the differences in timing of the SAO phases noted above. Moreover, the westward acceleration phase centred around December gradually descends with time, in contrast to MERRA2 where it appears simultaneously over an extended height region. In the difference plots (Figure 5e,f), at altitudes below 0.1 hPa the values are mostly negative during the SAOW periods, which suggests a weaker westerly forcing during this phase. The exception is the period of strong positive difference immediately before the westerly phase onset. Normally, this would suggest a greater eastward forcing in the model, but in this case, the discrepancy in timing is primarily responsible. For example, the WACCM eastward acceleration at 1 hPa starts almost a month before that in MERRA2 and this partly contributes to the strong positive value in the difference plot, since the reanalysis still has easterly acceleration at this time. Furthermore, during the rest of the westerly phase, the model fails to show sufficiently strong eastward acceleration, especially at altitudes between 1 and 5 hPa, resulting in the low magnitude of the westerly winds that was previously noted.

As described in Section 2, the forcing of the SAO can be analysed as a combination of four terms in the TEM equation: meridional advection, vertical advection, EP flux divergence and a residual term that includes GW forcing. We now examine each of these in detail to identify how they evolve over time and how the model differs from the reanalyses.

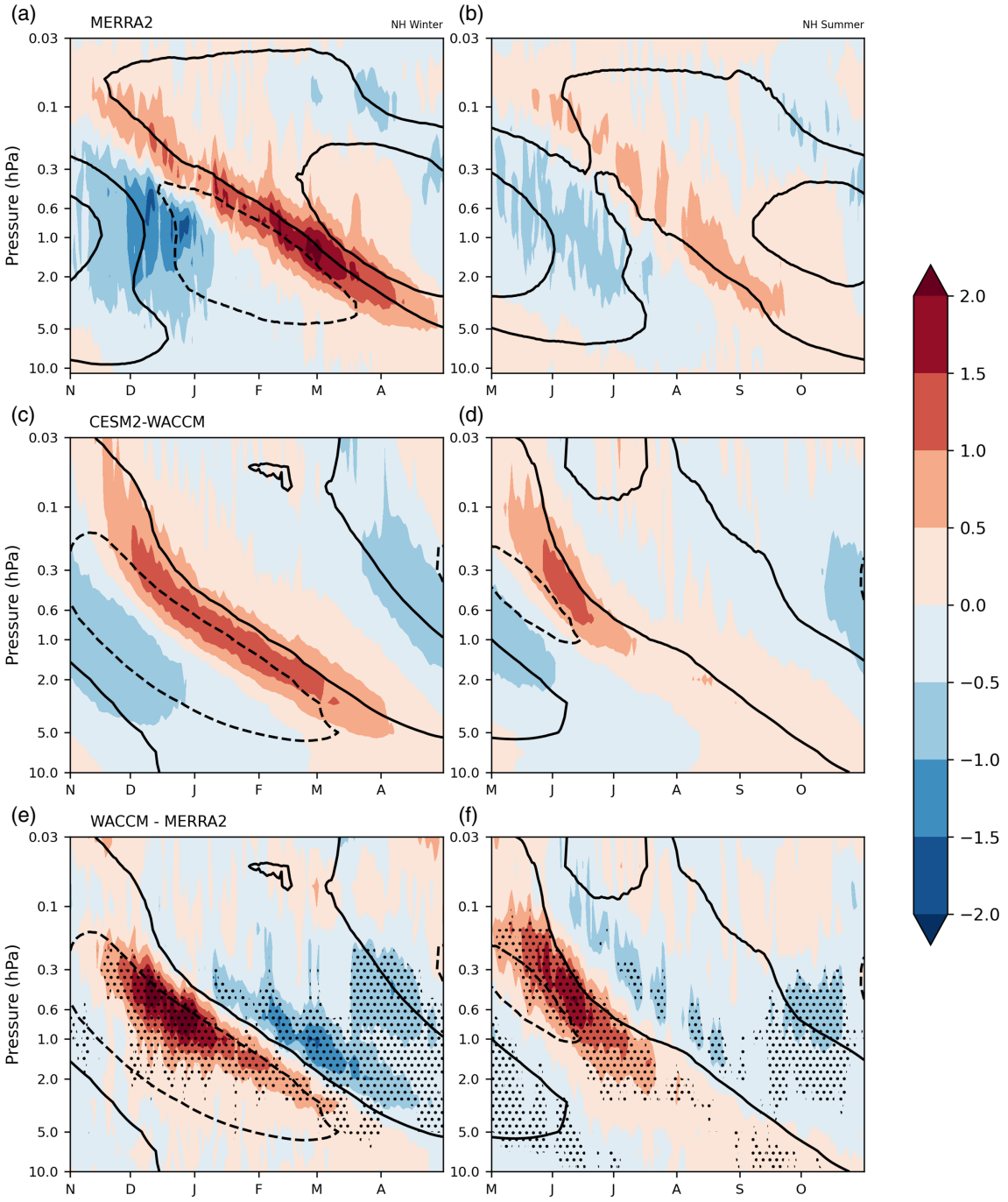

FIGURE 5 Climatology of zonal-mean zonal wind tendency ($m \cdot s^{-1} \cdot day^{-1}$) averaged over 5° N to 5° S for (a,b) Modern-Era Retrospective Analysis for Research and Applications, Version 2 (MERRA 2), (c,d) Whole Atmosphere Community Climate Model (WACCM), (e,f) WACCM minus MERRA2 differences. The respective climatological zonal-mean zonal wind contours of −20, 0, 20 $m \cdot s^{-1}$ are overlaid in (a–d) and the WACCM climatological zonal-mean zonal wind contours are overlaid in (e,f). Stippling denotes 99% confidence interval.

3.3.1 | Advection

Figure 6a,b shows the contribution of meridional advection in MERRA2 to the forcing of the SAO winds (first term on the RHS of Equation 1). The part of this term associated with the BDC advects easterlies from the summer hemisphere. The forcing increases with height above the stratopause and is strongest above ∼0.1 hPa, reflecting the GW-driven mean meridional circulation at those altitudes, with a secondary peak at ∼1 hPa centred around the solstice period. It is important to note that although there is GW-driven mean meridional circulation above

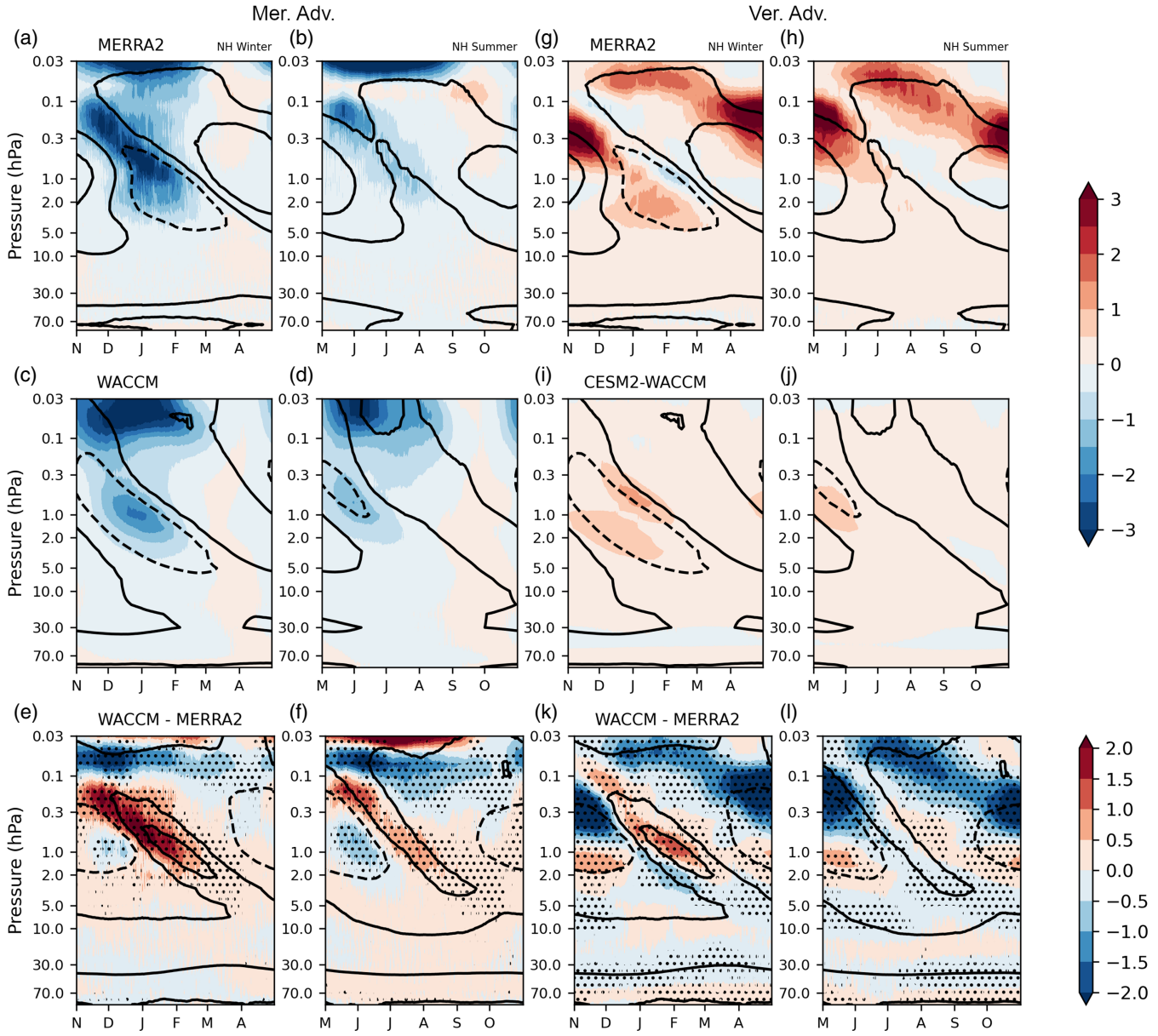

FIGURE 6 Climatology of zonal-mean zonal wind tendency due to meridional advection ($m \cdot s^{-1} \cdot day^{-1}$) averaged over 5° N to 5° S for (a,b) Modern-Era Retrospective Analysis for Research and Applications, Version 2 (MERRA 2), (c,d) Whole Atmosphere Community Climate Model (WACCM), (e,f) WACCM minus MERRA2 differences. Climatology of zonal-mean zonal wind tendency due to vertical advection ($m \cdot s^{-1} \cdot day^{-1}$) for (g,h) MERRA2, (i,j) WACCM, (k,l) WACCM minus MERRA2 differences. Corresponding zonal mean zonal wind contours of −20, 0, 20 $m \cdot s^{-1}$ are overlaid (a–d,g–j). Differences in zonal mean zonal wind contours of −20, 0, 20 $m \cdot s^{-1}$ are overlaid in e, f, k, l. Stippling denotes 99% confidence interval.

0.1 hPa, due to upper boundary conditions in MERRA2, the meridional advection above this altitude might not be realistic. The overlaid zonal-mean zonal wind contours in Figure 6 confirm that the westward forcing due to meridional advection matches very well the arrival of easterly winds of the SAO, as suggested by previous studies (Holton & Wehrbein, 1980). Even though there is a predominant easterly forcing pattern for the majority of the months appearing at all levels almost simultaneously (Figure 6a,b May and November), there is also evidence of descent in the peak forcing, for example between November and February in the height range 0.2–5 hPa.

The meridional advection pattern in WACCM (Figure 6c,d) is similar to that in MERRA2, but the magnitude is noticeably smaller. Despite the reduced magnitude of westward forcing due to meridional advection, WACCM nevertheless achieves realistic easterly SAO amplitudes since the intervening westerlies are also weaker. When compared to MERRA2 (Figure 6e,f) the westward forcing due to meridional advection in WACCM is stronger early

on at lower altitudes (Figure 6c,d at 1 hPa), which contributes to the early termination of the westerly phase in WACCM.

Weaker meridional advection in JJA compared with DJF is apparent in both MERRA2 and WACCM below 0.1 hPa. However, even though the earlier analysis shown in Figure 3 suggests that WACCM succeeds in capturing a reasonable annual cycle, the overall magnitude of advection is much weaker in WACCM, especially in DJF (as the difference plots in Figure 6e,f clearly show). Further analysis of the contributions to the horizontal advection term in Equation (1) was performed (see Figure S1) by separately examining the meridional residual circulation ($\overline{v}^*$) and meridional gradient of zonal mean zonal wind (du/dy). Differences in du/dy are a major contributor to the generally weaker magnitudes of meridional advection in WACCM compared to MERRA2. The figure also shows that while WACCM $\overline{v}^*$ during NH winter resembles that of MERRA2, it appears overly strong during SH winter. Consequently, WACCM does not capture the strong difference in magnitude of $\overline{v}^*$ between the NH and SH winter, which is evident in MERRA2. This shows that the anomalously weak annual cycle amplitude in WACCM horizontal advection is primarily due to the $\overline{v}^*$ term, suggesting that the well-known difference in midlatitude planetary wave breaking (or the role of GW driving) between the two hemispheres that produces a stronger BDC around January than July is not well simulated by WACCM.

Figure 6g,h shows the corresponding MERRA2 plots for the contribution of vertical advection (second term on the RHS of Equation (1)). In contrast to the meridional advection term, vertical advection is dominated by westerly forcing. The strength of the vertical advection consists of two contributions – the vertical advection associated with the large-scale BDC, and a more locally induced vertical circulation associated with in-situ equatorial wave forcing. The balance of the two contributions will vary both with height and with time of the year. The BDC is known to consist of upwelling at equatorial latitudes throughout the year, while locally induced circulations will produce upwelling during periods of westward wave forcing (negative vertical wind shear) and downwelling during periods of eastward wave forcing (positive vertical wind shear), thus maintaining approximate thermal wind balance. Thus, depending on the strength of the localised wave forcing (and the resulting induced circulation), there is likely to be weakened upwelling (or possibly even downwelling) at the onset of the SAOW and upwelling for the rest of the year.

The analysis of MERRA2 indicates that the primary effect of vertical advection is to produce a westerly acceleration, with peak forcing around 0.3 hPa just above the maximum westerlies at 1 hPa in April/May and in November (Figure 6g,h). This aligns with the start of the transition from the maximum westerly phase towards the easterly phase. Conversely, at the transition towards the westerly phase there is an opposing westward forcing, but it is much shorter-lived and weaker. These patterns are consistent with vertical advection driven by upwelling throughout the year. The presence of upwelling throughout the year was verified by examining the residual-mean vertical velocities $\overline{w}^*$ (Figure S2) which are positive, that is, consistent with upwelling throughout the year, but with decreased magnitude at both equinoxes. Upwelling at this height advects westerly winds from the peak westerlies at 1 hPa during the equinox periods (April/May and November) into the region around 0.3 hPa, where the greatest westerly forcing is seen in Figure 6g,h. This acts against the increasing easterly forcing, thus weakening and slowing the onset of the easterly phase. Similarly, upwelling during the solstice periods (Jan/Feb and July/August) advects easterlies from below, but the easterly SAO phase at 1 hPa in MERRA2 is relatively weak, so the forcing that would counteract the incoming westerly phase is correspondingly weak. These diagnostics demonstrate that vertical advection counteracts the SAO winds above 1 hPa and is particularly effective at slowing the onset of the easterly phase through advection of westerly winds from below. It is thus an important contribution to lengthening the westerly phase in the MERRA2 dataset, especially above 1 hPa.

The effect of vertical advection in WACCM (Figure 6i,j) is quite different from that in MERRA2. Despite the overall vertical advection forcing being eastward in WACCM, the timing and amplitude of the forcing are very different. Especially during the SAOW (at equinox), vertical advection forcing is virtually absent, thus failing to provide a forcing to help maintain the westerly phase of the modelled SAO at the upper levels (and this is confirmed by the difference plot – Figure 6k,l). This absence can be partly explained by the fact that the westerlies below the level of the peak SAO westerlies are much weaker in the model (Figure 6) and thus the vertical advection contribution is correspondingly weaker. This deficiency in vertical advection suggests one possible source for the easterly bias, especially above 1 hPa. However, the key to understanding this lack of vertical advection forcing lies in understanding the reason for the weaker westerlies at the lower levels. The presence of eastward forcing caused by vertical advection during the transition from easterly to westerly winds in DJF around 1 hPa and above is also rather unexpected when compared to the reanalysis. This observation suggests the occurrence of net downwelling during this period, advecting the westerly winds from 0.3 hPa or higher and this is confirmed by examination of the WACCM $\overline{w}^*$ fields (Figure S2). WACCM exhibits downwelling during May–June and November–February

above 1 hPa in contrast to MERRA2 which has upwelling all year round. The WACCM global-scale BDC upwelling thus appears to be weaker during equinox than the locally induced circulation due to the onset of the westerly SAO winds. This suggests that either the tropical upwelling component of the BDC above 1 hPa associated with midlatitude wave forcing is weaker in WACCM than in MERRA2, or the induced downwelling at the onset of the SAOW is larger in WACCM than in MERRA2. In the following section we explore this further and show that the net downwelling in WACCM at equinox is associated with GWD and its induced circulation.

In summary, horizontal advection is important in producing the easterly SAO phase at solstice and is also an important contribution to the observed annual cycle because of the hemispheric asymmetry in planetary wave driving and BDC strength. Compared with MERRA2, the modelled WACCM horizontal advection forcing is weak at SAO altitudes. Vertical advection mostly acts as counteracting force at levels above the peak of the SAO winds, since upwelling from below throughout the year advects winds whose sign opposes that of the incoming SAO phase. In MERRA2, vertical advection in this way plays an important role in perpetuating the equinoctial westerlies in the region above 1 hPa, since the winds below this level are predominantly westerly. In WACCM this vertical advection forcing is missing, which suggests that the model lacks an important contribution to the westerlies above 1 hPa.

3.3.2 | Resolved wave forcing

The resolved wave forcing is examined using the EP flux divergence term in Equation (1), shown in Figure 7a–f. The major feature of the resolved wave forcing in WACCM (Figure 7c,d) is the dominance of westward wave forcing, which is presumably due to Rossby waves propagating into the region from midlatitudes and/or tropical inertia-GWs. MERRA2, on the other hand, shows eastward forcing as well as westward forcing. The eastward forcing is present particularly in NH winter along the westerly shear zones as the winds transition from easterlies to westerlies, which is consistent with (but does not demonstrate) wave breaking at critical layers (Pahlavan et al., 2021). It indicates that resolved waves contribute to the SAOW in MERRA2 but the WACCM fails to capture this contribution.

To explore this further, a wavenumber frequency spectral analysis of the daily zonal winds from 5° N to 5° S was conducted using the method outlined in Wheeler and Kiladis (1999). Since we are interested in wave forcing of the SAOW, we focus on the symmetric power spectra quantifying the Kelvin waves. The symmetric power spectrum is calculated using zonal wind anomalies symmetric with respect to equator, separated into 96-day windows with two-month overlap (for a detailed description of wavenumber frequency power spectra calculations, see Wheeler and Kiladis, 1999). Figure 8 shows the symmetric wavenumber frequency power spectra of the zonal wind summed over 5° N–5° S at 10 hPa, 5 hPa and 1 hPa level normalised by the background power. In the difference plots, Figure 8c,f,i, the difference between WACCM and MERRA2 raw power spectra, without normalising with respect to the background, is shown. This obviates problems that might arise from differences in the background power between WACCM and MERRA2. Negative wavenumbers correspond to westward-propagating waves and positive wavenumbers correspond to eastward-propagating waves. Hirota (1978) noted that Kelvin waves of 10-day period play a crucial role in reversing the SAO winds from easterly to westerly. Superimposed in Figure 8 are the theoretical dispersion curves for Kelvin waves (positive wavenumbers) and Rossby waves (negative wavenumbers). The plot immediately confirms that the Kelvin waves reaching the stratopause in the MERRA2 analysis are of relatively high-phase speed ($\sim 45\,\mathrm{m\cdot s^{-1}}$, i.e., between dispersion curves of equivalent depth 100 and 400), as expected. The increasing slope of the Kelvin wave power spectra in MERRA2 as we move up from 10 to 1 hPa confirms the filtering of slower waves at lower altitudes. The WACCM power spectra show similar changes with pressure but the Kelvin wave power in WACCM at fast-phase speeds is considerably weaker than in MERRA2 at 1 hPa. In fact, at all altitudes shown, Kelvin wave power in WACCM is significantly weaker compared to MERRA2 (Figure 8c,f,i), which is consistent with the reduced westerly forcing at these altitudes.

The spectra also indicate power in the westward-propagating wave region. MERRA2 and WACCM have spectral peaks at lower wavenumbers (less than 3) of periodicities 10–20 days and 5–6 days at all presented altitudes (Figure 8a–i). These are wave modes often observed at midlatitudes, indicating westward forcing by extratropical travelling Rossby waves (Salby, 1984). At 1 hPa (as shown in Figure 8a,b), a notable contribution is evident at wavenumbers 3 and 4, exhibiting a frequency range of 0.4–0.5 cycles per day (cpd). Earlier studies suggest that these wavenumber and frequency range align with the two-day waves frequently observed in the mesosphere during solstices originating from jet instabilities (Ern et al., 2013; Plumb, 1983). However, wavenumber 3, two-day waves are documented to be a Rossby-gravity (RG) wave mode, which is not expected to show up in the symmetric zonal wind spectrum near the equator. Further

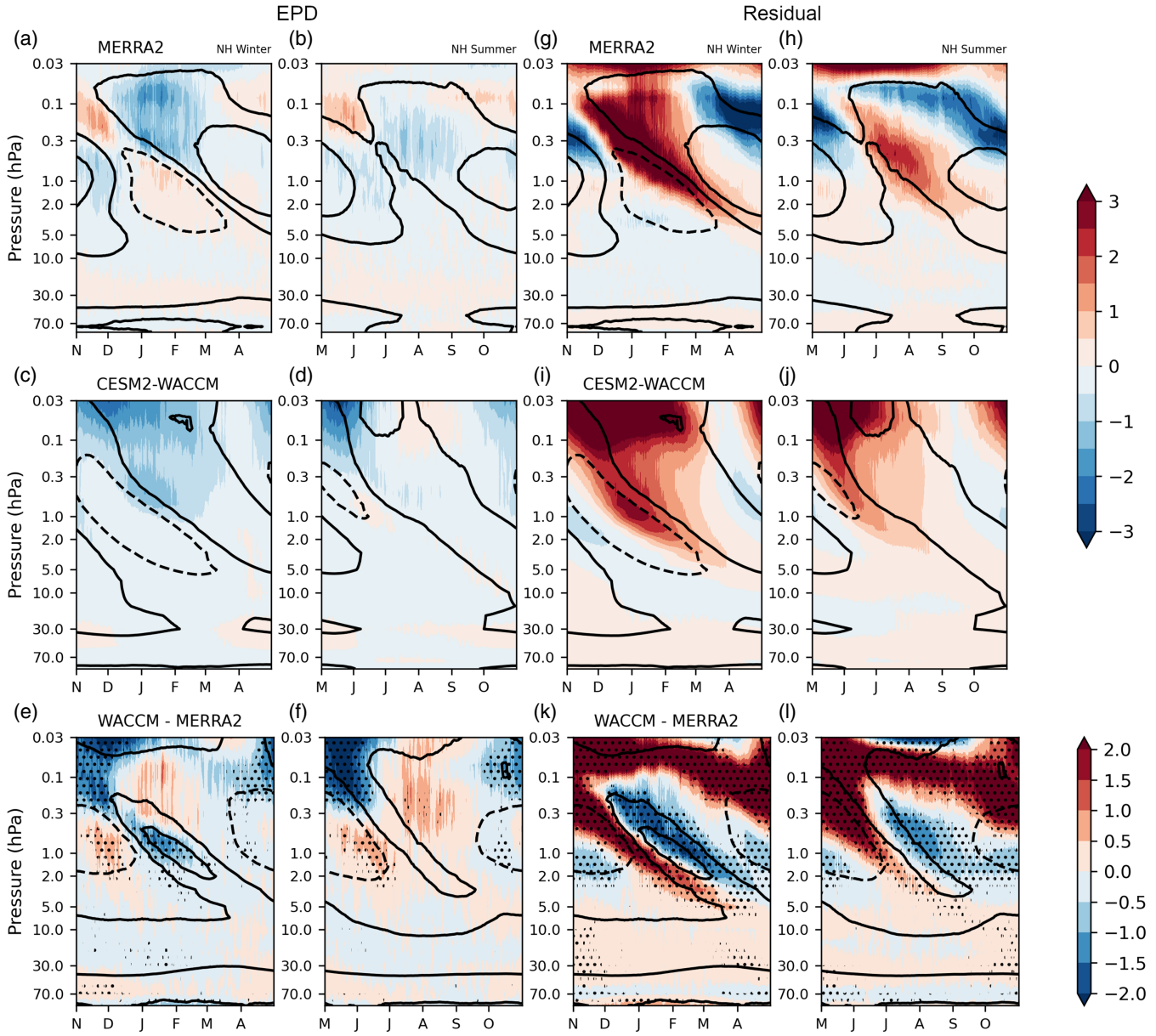

FIGURE 7 Climatology of zonal-mean zonal wind tendency due to Eliassen Palm (EP) flux divergence ($m \cdot s^{-1}$ day^{-1}) averaged over 5° N to 5° S for (a,b) Modern-Era Retrospective Analysis for Research and Applications, Version 2 (MERRA 2), (c,d) Whole Atmosphere Community Climate Model (WACCM), (e,f) WACCM minus MERRA2 differences. Climatology of zonal-mean zonal wind tendency due to the residual term in Equation (1) ($m \cdot s^{-1} \cdot day^{-1}$) for (g,h) MERRA2, (i,j) WACCM, (k,l) WACCM minus MERRA2 differences. Corresponding zonal mean zonal wind contours of −20, 0, 20 $m \cdot s^{-1}$ are overlaid (a–d,g–j). Differences in zonal mean zonal wind contours of −20, 0, 20 $m \cdot s^{-1}$ are overlaid in e, f, k, l. Stippling denotes 99% confidence interval.

analysis showed that barotropic instability is present at 1 hPa during solstices (Figure S3) which suggests that the instability likely excites a broad spectrum of waves such that the zonal wind velocity pattern of RG waves near the equator is altered. The strength and position of regions of barotropic instability slightly differs between WACCM and MERRA2, which can be attributed to the difference in jet characteristics. The stronger EP flux convergence and divergence near regions of weaker negative barotropic vorticity gradient that are seen in the figure are consistent with waves acting to reduce the instability (e.g., Figure S3 JJA). Figure S3 confirms that EP flux divergence close to equator has components of Rossby waves propagating from midlatitudes, and in-situ waves generated at instability. Further exploration of these waves is outside the scope of this current study, especially since Figure 7 indicates that the resolved wave contribution to SAO is much weaker than the residual term in both datasets.

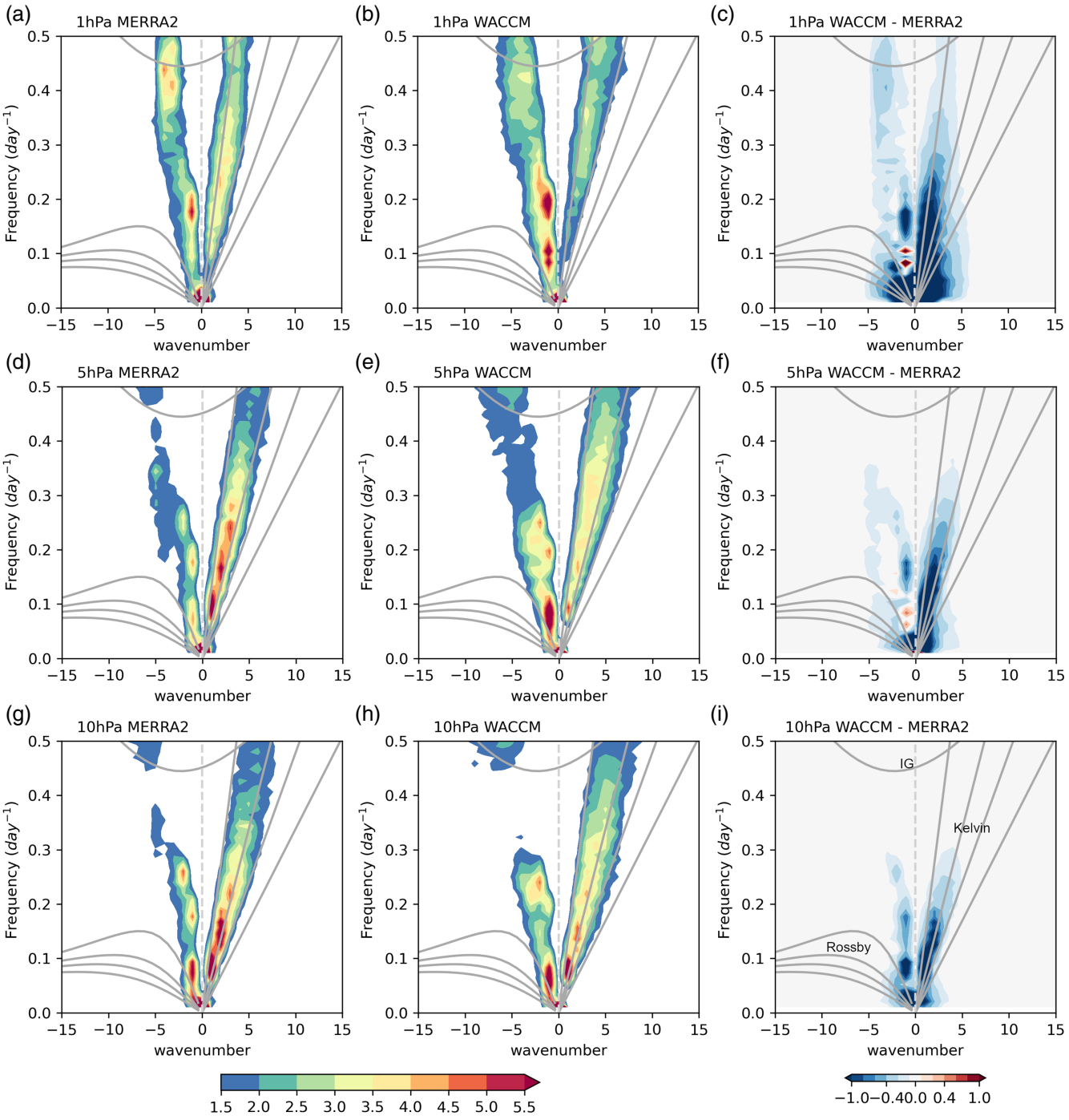

FIGURE 8 Wavenumber–frequency power spectra of the symmetric component of zonal-mean zonal wind normalised by the background power at 1 hPa, 5 hPa and 10 hPa for (a,d,g) Modern-Era Retrospective Analysis for Research and Applications, Version 2 (MERRA2) and (b,e,h) Whole Atmosphere Community Climate Model (WACCM). The overlaid dispersion curves correspond to shallow-water Kelvin waves and Rossby waves of equivalent depth 25, 50, 100 and 400 m, as identified in panel (i). WACCM minus MERRA2 differences between raw symmetric power spectra ($m^2 \cdot s^{-2}$) are shown in panels c, f and i.

3.3.3 | Gravity wave forcing

To obtain a complete picture of the wave driving we also need to examine the parameterised GWD. The MERRA2 GWD data are only available up to 0.1 hPa. For this reason, we employ the methodology similar to Ern et al. (2021) and calculate the residual term by subtracting all three previous forcing terms from the total rate of change of zonal-mean zonal wind (Figure 7g–j). For MERRA2, this residual term will include parameterised GW forcing and

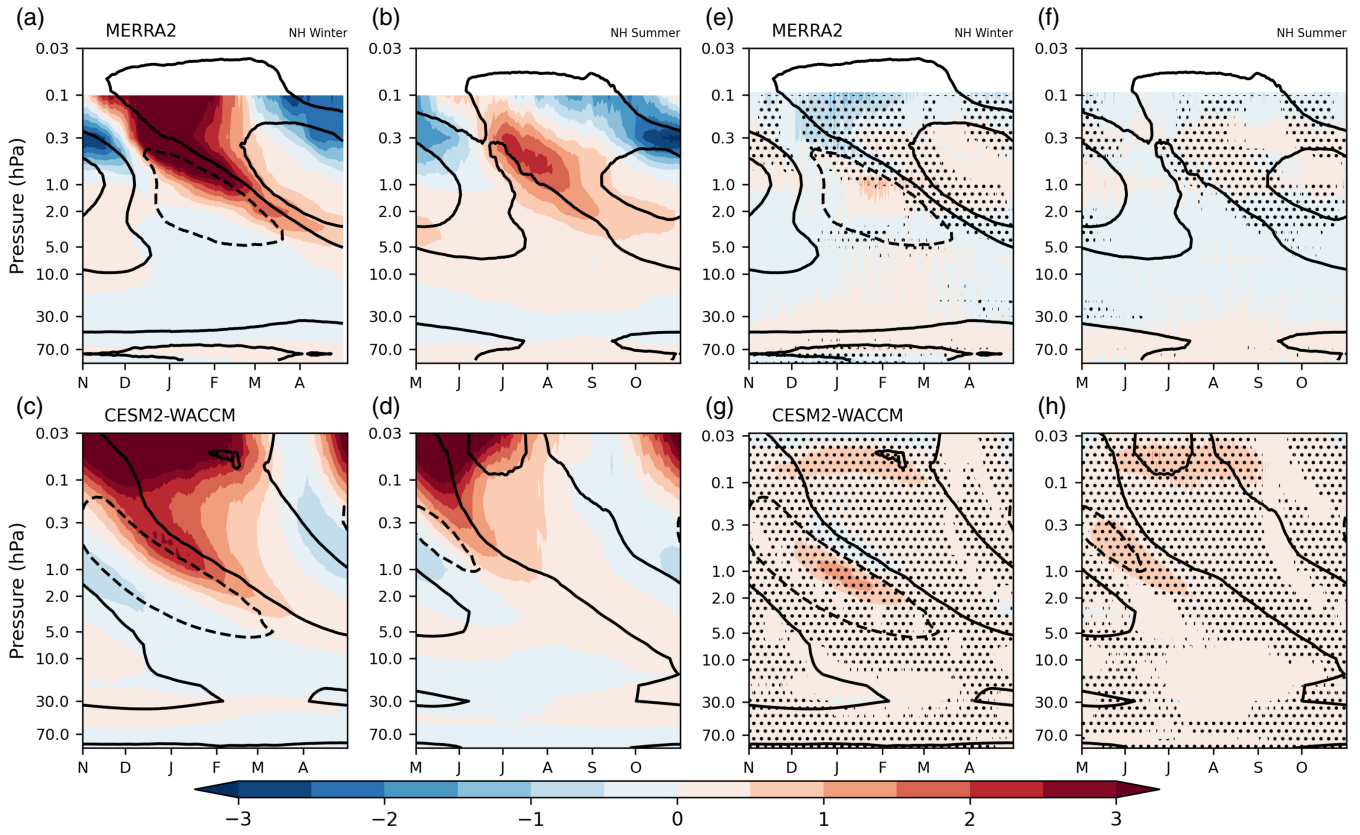

FIGURE 9 Climatology of zonal-mean zonal wind tendency due to gravity wave drag ($m \cdot s^{-1} \cdot day^{-1}$) averaged over 5° N to 5° S for (a,b) Modern-Era Retrospective Analysis for Research and Applications, Version 2 (MERRA2) and (c,d) Whole Atmosphere Community Climate Model (WACCM). Difference between residual term ($m \cdot s^{-1} \cdot day^{-1}$) and zonal-mean zonal wind tendency due to GWD for (e,f) MERRA 2 and (g,h) WACCM. Corresponding zonal- mean zonal wind contours of −20, 0, 20 $m \cdot s^{-1}$ are overlaid. Stippling denotes 99% confidence interval.

analysis increments, while for WACCM this term will include GW forcing and other effects such as numerical diffusion, associated with the dynamical core. In Figure 9e–h, we show the difference between residual terms (Figure 7g–j) and parameterised GWD (Figure 9a–d) at equatorial latitudes in both MERRA2 and WACCM. The differences in both datasets demonstrate that the residual term primarily consists of GWD. The differences are almost negligible apart from certain regions, for example, in January between 1 and 2 hPa in WACCM (Figure 9g). Thus, we will consider the residual term as GWD in this study, diverging from the approach in Ern et al., 2021, where EP flux divergence with wavenumbers exceeding 20 is incorporated to residual term to define GWD.

The residual (GWD) term derived in this way, shown in Figure 7g–l, indicates that in MERRA2, GWD plays a major role in the initiation of both the westerly and easterly SAO phases. The westward GW forcing is, however, slightly weaker than the eastward forcing and is confined to heights above 0.6 hPa. Recent studies using satellite data have highlighted that, at the source level and in the lower stratosphere near the equator, the eastward convective GW momentum flux is larger than its westward component (Lee et al., 2022; Liu et al., 2022). This observation implies a diminished availability of momentum for westward forcing. In addition, the easterly phase of the QBO has larger amplitude and hence there will be more filtering of westward GWs at lower altitudes. These two factors contribute to the weaker westward GW forcing seen in Figure 7g–l. The GW forcing (of either sign) generally appears where the vertical wind shears are strongest and strengthens the respective phase further by providing momentum forcing in the same direction. Figure 7g,h confirms that the transition between SAO phases coincides with the peak of GW forcing, making it an important component in forcing the SAO in MERRA2.

In the case of WACCM Figures 7 and 9 suggest that GW plays a major role in the initiation of the westerly phase only, although as indicated by the difference plot (Figure 7k,l), the model does not reproduce correctly the strength and timing of this forcing. As noted previously, the modelled easterly phase starts to weaken slightly too soon, consistent with the early weakening of

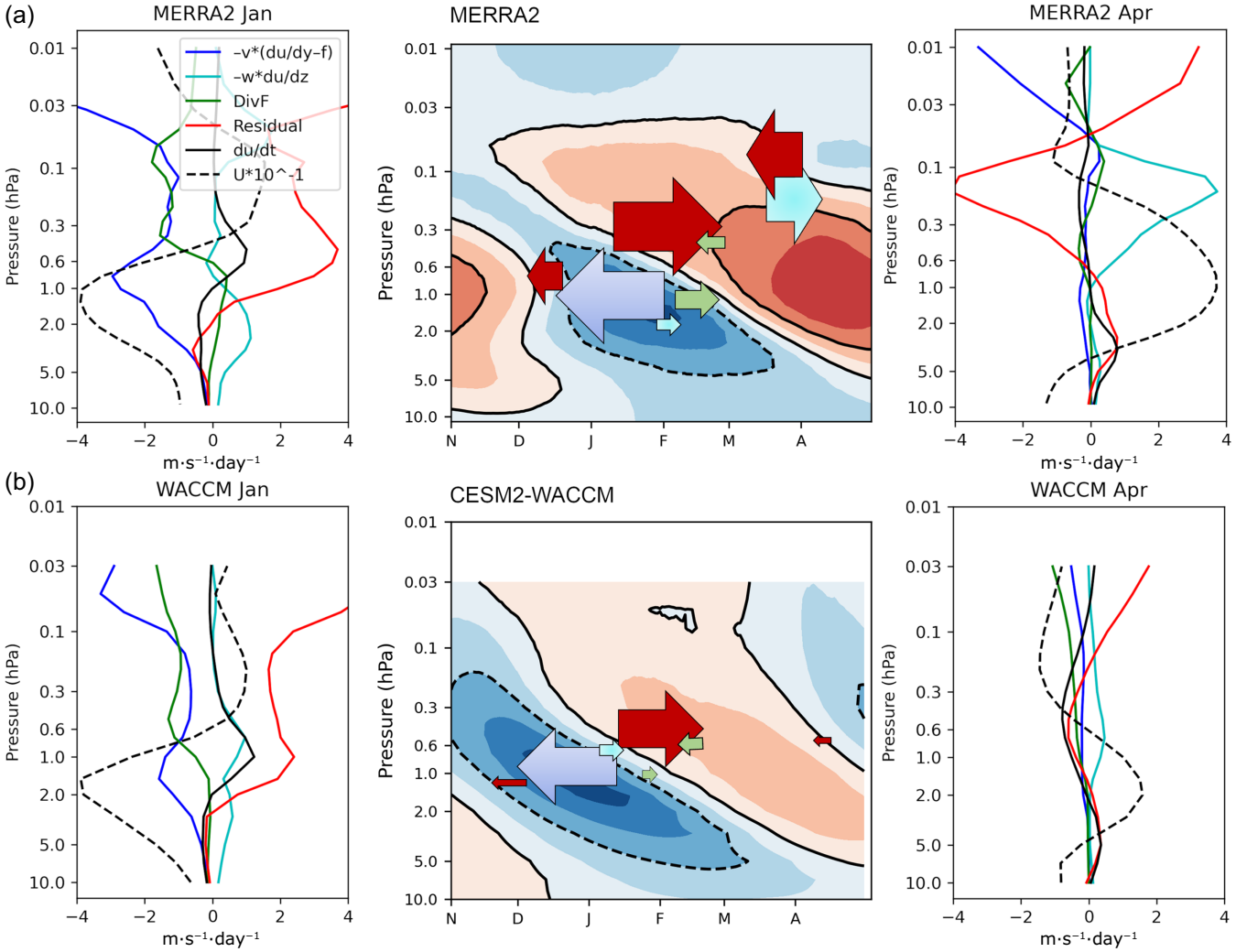

FIGURE 10 Schematic summarising the different forcing terms acting on the semi-annual oscillation westerly and easterly phases of (a) Modern-Era Retrospective Analysis for Research and Applications, Version 2 (MERRA2) and (b) Whole Atmosphere Community Climate Model (WACCM). The arrows in the middle column plots represent different forcing terms with colours that correspond to those in the line plots. Forward arrows indicate eastward forcing and backward arrows indicate westward forcing. The length and width of the arrows roughly indicate the relative duration and strength of the forcing. The line plots represent the amplitude of each of the forcing terms in (left) January and (right) April.

the meridional advection forcing, so the eastward GW forcing starts sooner. Since the GWD parameterisation also depends on the vertical gradient of the wind, some of this inconsistency in timing and strength could also be associated with the slightly lower vertical resolution of this version of WACCM compared with MERRA2 so that it cannot represent sharp vertical gradients so well. However, while Garcia and Richter (2019) have shown that a version of WACCM with improved vertical resolution (110 levels) can produce a much better QBO than the version analysed here, the impact of improved resolution was primarily on the resolved waves rather than on the parameterised GWD.

An interesting side note here is that the timing of occurrence of GW forcing in WACCM exactly matches the downwelling described earlier in the vertical advection analysis. This suggests that the stronger downwelling at equinox in WACCM compared to the reanalysis is indeed caused by the eastward forcing due to GW. If this is the case, this could also explain the reduced vertical advection of westerlies during the SAOWs in WACCM. Since there is a lack of strong westward GWD at this time, there is no induced upwelling, thus failing to provide the strong westerly wind advection from lower levels (Figure 6i,j). In contrast, we note that in MERRA2, the westward forcing due to GWD and the eastward forcing associated with vertical advection occur around the same time. Because of this, they almost cancel each other in MERRA2 so there is roughly no net westerly forcing due to vertical advection after the westerly wind maxima of each SAOW, similar to WACCM (Figure 6i,j). This implies that the weakened resolved

Kelvin waves and weakened eastward parameterised GWs likely play a more important role in the weakening of the SAOW in WACCM than the vertical advection deficiencies.

In summary, both GWD and resolved wave forcing contribute to the SAOW transitioning in MERRA2 and mostly act to reinforce each other, although the GWD is clearly the dominant contribution. In WACCM, however, the eastward wave forcing is driven almost entirely by the GWs since the resolved eastward wave forcing is substantially underestimated. The MERRA2 analysis also suggests a contribution to the easterly SAO phase from the GWs, but this contribution is much weaker in WACCM.

4 | SUMMARY

A comparison of how the SAO is forced in MERRA2 and WACCM has been performed by examining the different forcing terms in the TEM, to identify possible reasons for the common easterly bias in climate models. The results are summarised by a schematic (Figure 10) that highlights the dominant forcing terms and their relative roles in forcing the SAO.

In MERRA2, the westerly phase of the SAO is initiated by the combined forcing from both resolved waves (EP flux divergence term) and GWs (residual term). The resolved waves primarily contribute to weakening of the existing easterly phase, while the GWs act to accelerate the new westerly phase in its first 1–2 months. Once the SAOW begins, the resolved waves then act to weakly oppose the flow. Since the net residual circulation in MERRA2 near the equator is upward throughout the year, once the SAO is well established the vertical advection term additionally advects westerlies from below which helps to maintain and strengthen the SAOW at the upper levels (although we note that the maximum amplitude of this term in MERRA2 is at 0.2 hPa where the reanalysis is considered less reliable). Nevertheless, the eastward GW forcing eventually weakens at the upper levels due to wave absorption below, and the upper-level flow slowly starts to decelerate, beginning to create an easterly shear zone at the higher altitudes. Thus, in the second half of the SAOW, strong westward forcing from GWs occurs, which acts to further weaken the westerly winds at the higher altitudes. Eventually the westward GW and meridional advection weaken the flow sufficiently, thus facilitating the shift to the easterly SAO phase. In summary, while GWD provides the largest SAO westerly forcing in MERRA2, the resolved waves and vertical advection also contribute to its strength and evolution.

In contrast, while GWD initiates the SAOW in WACCM, it is weaker and dies out sooner than in MERRA2. Contributions from the resolved waves are weak and do not play any appreciable role in the initiation stage. Once the SAOW starts, the resolved waves counteract the eastward GWD forcing and thus reduce the westerly wind's magnitude. The vertical advection contribution to maintaining the westerly phase at the upper levels is also absent, because there is net downwelling at the equator during equinox.

In the case of the easterly SAO phase, the meridional advection and GW forcing both play major roles in MERRA2. The resolved wave forcing helps to weaken the westerly phase but does not contribute much once the easterly phase starts. Vertical advection, however, weakly opposes this phase. The greater GW westward forcing and meridional advection in DJF compared to JJA contributes to the annual cycle in the SAO easterly phase. In WACCM, even though most of the relevant forcings are slightly weaker than in MERRA2, the model is more successful in reproducing the easterly phase of SAO and its forcings compared to the westerly phase. The weaker vertical advection noted earlier (see Figure S2) also points to a weaker BDC upwelling above 1 hPa than in MERRA2.

In conclusion, our study suggests that increased westerly forcing from both resolved waves and GWs at SAO altitudes would help to improve the SAO representation in WACCM and correct the easterly bias. There are several possible routes by which this could be achieved. The generation of Kelvin waves within the troposphere could possibly be deficient due to inaccuracies in the temporal or spatial variability of tropical convective activity. Increased horizontal and vertical resolution would make it possible to better resolve and improve the vertical propagation of resolved waves and improved resolution of vertical gradients could also help to increase the GW forcing. It might also help to refine the GW parameterisation scheme to increase the magnitude of higher phase speed waves that can reach up to the upper stratosphere. Nevertheless, we note that these results are based on a comparison with MERRA2 reanalysis and there are still many uncertainties in observations and reanalyses in the upper stratosphere, especially at equatorial latitudes (Ch 11, SPARC, 2022).

ACKNOWLEDGEMENTS

Aleena M. Jaison is thankful for Oxford-Richards Graduate Scholarship for supporting this research. Lesley J. Gray and Scott Osprey acknowledge funding from the Natural Environment Research Council (NERC) through its funding of the National Centre for Atmospheric Science (NCAS). This material is based upon work supported by the NSF National Center for Atmospheric Research, which is a major facility sponsored by the US National Science Foundation under Cooperative Agreement No.1852977.

CONFLICT OF INTEREST STATEMENT

The authors declare no conflicts of interest.

DATA AVAILABILITY STATEMENT

MERRA2 datasets used in this study are available at Global Modeling and Assimilation Office (GMAO) (2015), MERRA-2 tavg3_3d_asm_Nv: 3d, 3-Hourly, Time-Averaged, Model-Level, Assimilation, Assimilated Meteorological Fields V5.12.4, Greenbelt, MD, USA, Goddard Earth Sciences Data and Information Services Center (GES DISC), Accessed: [November 2022], 10.5067/SUOQESM06LPK, and at Global Modeling and Assimilation Office (GMAO) (2015), MERRA-2 tavg3_3d_udt_Np: 3d, 3-Hourly, Time-Averaged, Pressure-Level, Assimilation, Wind Tendencies V5.12.4, Greenbelt, MD, USA, Goddard Earth Sciences Data and Information Services Center (GES DISC), Accessed: [November 2022], 10.5067/CWV0G3PPPWFW. CESM2-WACCM datasets used in this study can be found at Danabasoglu, Gokhan (2019). NCAR CESM2-WACCM output prepared for CMIP6 CMIP piControl. Version 20190917[1]. Earth System Grid Federation. https://doi.org/10.22033/ESGF/CMIP6.10094. ERA5 (Hersbach et al. (2017): Complete ERA5 from 1940: Fifth generation of ECMWF atmospheric reanalyses of the global climate. Copernicus Climate Change Service (C3S) Data Store (CDS). DOI: 10.24381/cds.143582cf (Accessed on 07-11-2022)) and ERA-interim data are available from the European Centre for Medium-Range Weather Forecasts (ECMWF).

ORCID

Aleena M. Jaison https://orcid.org/0009-0006-5613-216X
Scott Osprey https://orcid.org/0000-0002-8751-1211
Anne K. Smith https://orcid.org/0000-0003-2384-5033

REFERENCES

Andrews, D.G., Holton, J.R. & Leovy, C.B. (1987) Chapter 3 – basic dynamics. In: Andrews, D.G., Holton, J.R. & Leovy, C.B. (Eds.) *Middle atmosphere dynamics*, Vol. 40. San Diego, CA: Academic Press, pp. 113–149.

Anstey, J.A., Osprey, S.M., Alexander, J., Baldwin, M.P., Butchart, N., Gray, L. et al. (2022) Impacts, processes and projections of the quasi-biennial oscillation. *Nature Reviews Earth and Environment*, 3, 588–603. Available from: https://doi.org/10.1038/s43017-022-00323-7

Anstey, J.A. & Shepherd, T.G. (2014) High-latitude influence of the quasi-biennial oscillation. *Quarterly Journal of the Royal Meteorological Society*, 140, 1–21. Available from: https://doi.org/10.1002/qj.2132

Baldwin, M.P., Gray, L.J., Dunkerton, T.J., Hamilton, K., Haynes, P.H., Randel, W.J. et al. (2001) The quasi-biennial oscillation. *Reviews of Geophysics*, 39, 179–229. Available from: https://doi.org/10.1029/1999RG000073

Butler, A.H., Arribas, A., Athanassiadou, M., Baehr, J., Calvo, N., Charlton-Perez, A. et al. (2016) The climate-system historical forecast project: do stratosphere-resolving models make better seasonal climate predictions in boreal winter? *Quarterly Journal of the Royal Meteorological Society*, 142, 1413–1427. Available from: https://doi.org/10.1002/qj.2743

Danabasoglu, G. (2019) *NCAR CESM2-WACCM model output prepared for CMIP6 CMIP historical*, Available from: https://doi.org/10.22033/ESGF/CMIP6.10071

Danabasoglu, G., Lamarque, J.F., Bacmeister, J., Bailey, D.A., DuVivier, A.K., Edwards, J. et al. (2020) The community earth system model version 2 (CESM2). *J Adv Model Earth Syst*, 12, e2019MS001916. Available from: https://doi.org/10.1029/2019MS001916

Danabasoglu, G., Lawrence, D., Lindsay, K., Lipscomb, W. & Strand, G. (2019) NCAR CESM2 model output prepared for CMIP6 CMIP piControl. https://doi.org/10.22033/ESGF/CMIP6.7733

Dee, D.P., Uppala, S.M., Simmons, A.J., Berrisford, P., Poli, P., Kobayashi, S. et al. (2011) The ERA-interim reanalysis: configuration and performance of the data assimilation system. *Quarterly Journal of the Royal Meteorological Society*, 137, 553–597. Available from: https://doi.org/10.1002/qj.828

Delisi, D.P. & Dunkerton, T.J. (1988) Seasonal variation of the semiannual oscillation. *Journal of Atmospheric Sciences*, 45, 2772–2787. Available from: https://doi.org/10.1175/1520-0469(1988)045<2772:SVOTSO>2.0.CO;2

Dunkerton, T. (1979) On the role of the kelvin wave in the westerly phase of the semiannual zonal wind oscillation. *Journal of Atmospheric Sciences*, 36, 32–41. Available from: https://doi.org/10.1175/1520-0469(1979)036<0032:OTROTK>2.0.CO;2

Dunkerton, T.J. (1981) On the inertial stability f the equatorial middle atmosphere. *Journal of Atmospheric Sciences*, 38, 2354–2364. Available from: https://doi.org/10.1175/1520-0469(1981)038<2354:OTISFT>2.0.CO;2

Dunkerton, T.J. & Delisi, D.P. (1997) Interaction of the quasi-biennial oscillation and stratopause semiannual oscillation. *Journal of Geophysical Research: Atmospheres*, 102, 26107–26116. Available from: https://doi.org/10.1029/96JD03678

Ebdon, R.A. (1975) The quasi-biennial oscillation and its association with tropospheric circulation pattern. *Meteor Mags*, 104, 282–297.

Ern, M., Preusse, P., Diallo, M., Preusse, P., Mlynczak, M.G., Schwartz, M.J. et al. (2021) The semiannual oscillation (SAO) in the tropical middle atmosphere and its gravity wave driving in reanalyses and satellite observations. *Atmospheric Chemistry and Physics*, 21, 13763–13795. Available from: https://doi.org/10.5194/acp-21-13763-2021

Ern, M., Preusse, P., Kalisch, S., Kaufmann, M. & Riese, M. (2013) Role of gravity waves in the forcing of quasi two-day waves in the mesosphere: an observational study. *Journal of Geophysical Research: Atmospheres*, 118, 3467–3485. Available from: https://doi.org/10.1029/2012JD018208

Ern, M., Preusse, P. & Riese, M. (2015) Driving of the SAO by gravity waves as observed from satellite. *Annales de Geophysique*, 33, 483–504. Available from: https://doi.org/10.5194/angeo-33-483-2015

Eyring, V., Bony, S., Meehl, G.A., Senior, C.A., Stevens, B., Stouffer, R.J. et al. (2016) Overview of the coupled model Intercomparison

project phase 6 (CMIP6) experimental design and organization. *Geoscientific Model Development*, 9, 1937–1958. Available from: https://doi.org/10.5194/gmd-9-1937-2016

Garcia, R.R. (2000) The role of equatorial waves in the semiannual oscillation of the middle atmosphere. Atmospheric Science Across the Stratopause, American Geophysical Union (AGU), 161–176.

Garcia, R.R. & Boville, B.A. (1994) "Downward control" of the mean meridional circulation and temperature distribution of the polar winter stratosphere. *Journal of Atmospheric Sciences*, 51, 2238–2245. Available from: https://doi.org/10.1175/1520-0469(1994)051<2238:COTMMC>2.0.CO;2

Garcia, R.R., Dunkerton, T.J., Lieberman, R.S. & Vincent, R.A. (1997) Climatology of the semiannual oscillation of the tropical middle atmosphere. *Journal of Geophysical Research: Atmospheres*, 102, 26019–26032. Available from: https://doi.org/10.1029/97JD00207

Garcia, R.R. & Richter, J.H. (2019) On the momentum budget of the quasi-biennial oscillation in the whole atmosphere community climate model. *Journal of the Atmospheric Sciences*, 76, 69–87. Available from: https://doi.org/10.1175/JAS-D-18-0088.1

Garfinkel, C.I. & Hartmann, D.L. (2011) The influence of the quasi-biennial oscillation on the troposphere in winter in a hierarchy of models. Part I: simplified dry GCMs. *Journal of the Atmospheric Sciences*, 68, 1273–1289. Available from: https://doi.org/10.1175/2011JAS3665.1

Gelaro, R., McCarty, W., Suárez, M.J., Todling, R., Molod, A., Takacs, L. et al. (2017) The modern-era retrospective analysis for research and applications, version 2 (MERRA-2). *Journal of Climate*, 30, 5419–5454. Available from: https://doi.org/10.1175/JCLI-D-16-0758.1

Gerber, E.P. & Manzini, E. (2016) The dynamics and variability model Intercomparison project (DynVarMIP) for CMIP6: assessing the stratosphere–troposphere system. *Geoscientific Model Development*, 9, 3413–3425. Available from: https://doi.org/10.5194/gmd-9-3413-2016

Gettelman, A., Mills, M.J., Kinnison, D.E., Garcia, R.R., Smith, A.K., Marsh, D.R. et al. (2019) The whole atmosphere community climate model version 6 (WACCM6). *Journal of Geophysical Research: Atmospheres*, 124, 12380–12403. Available from: https://doi.org/10.1029/2019JD030943

Gray, L.J., Anstey, J.A., Kawatani, Y., Lu, H., Osprey, S. & Schenzinger, V. (2018) Surface impacts of the quasi biennial oscillation. *Atmospheric Chemistry and Physics*, 18, 8227–8247. Available from: https://doi.org/10.5194/acp-18-8227-2018

Gray, L.J., Brown, M.J., Knight, J., Andrews, M., Lu, H., O'Reilly, C. et al. (2020) Forecasting extreme stratospheric polar vortex events. *Nature Communications*, 11, 4630. Available from: https://doi.org/10.1038/s41467-020-18299-7

Gray, L.J., Crooks, S., Pascoe, C., Sparrow, S. & Palmer, M. (2004) Solar and QBO influences on the timing of stratospheric sudden warmings. *Journal of the Atmospheric Sciences*, 61, 2777–2796. Available from: https://doi.org/10.1175/JAS-3297.1

Gray, L.J., Lu, H., Brown, M.J., Knight, J.R. & Andrews, M.B. (2022) Mechanisms of influence of the semi-annual oscillation on stratospheric sudden warmings. *Quarterly Journal of the Royal Meteorological Society*, 148, 1223–1241. Available from: https://doi.org/10.1002/qj.4256

Gray, L.J. & Pyle, J.A. (1986) The semi-annual oscillation and equatorial tracer distributions. *Quarterly Journal of the Royal Meteorological Society*, 112, 387–407. Available from: https://doi.org/10.1002/qj.49711247207

Gray, L.J. & Pyle, J.A. (1989) A two-dimensional model of the quasi-biennial oscillation of ozone. *Journal of Atmospheric Sciences*, 46, 203–220. Available from: https://doi.org/10.1175/1520-0469(1989)046<0203:ATDMOT>2.0.CO;2

Hamilton, K. & Mahlman, J.D. (1988) General circulation model simulation of the semiannual oscillation of the tropical middle atmosphere. *Journal of Atmospheric Sciences*, 45, 3212–3235. Available from: https://doi.org/10.1175/1520-0469(1988)045<3212:GCMSOT>2.0.CO;2

Hersbach, H., Bell, B., Berrisford, P., Hirahara, S., Horányi, A., Muñoz-Sabater, J. et al. (2017) Complete ERA5 from 1940: Fifth generation of ECMWF atmospheric reanalyses of the global climate. *Copernicus Climate Change Service (C3S) Data Store (CDS)*. Available from: https://doi.org/10.24381/cds.143582cf

Hersbach, H., Bell, B., Berrisford, P., Hirahara, S., Horányi, A., Muñoz-Sabater, J. et al. (2020) The ERA5 global reanalysis. *Quarterly Journal of the Royal Meteorological Society*, 146, 1999–2049. Available from: https://doi.org/10.1002/qj.3803

Hirota, I. (1978) Equatorial waves in the upper stratosphere and mesosphere in relation to the semiannual oscillation of the zonal wind. *Journal of Atmospheric Sciences*, 35, 714–722. Available from: https://doi.org/10.1175/1520-0469(1978)035<0714:EWITUS>2.0.CO;2

Hirota, I. (1980) Observational evidence of the semiannual oscillation in the tropical middle atmosphere—a review. *Pure and Applied Geophysics*, 118, 217–238. Available from: https://doi.org/10.1007/BF01586452

Hitchman, M.H. & Leovy, C.B. (1986) Evolution of the zonal mean state in the equatorial middle atmosphere during October 1978-may 1979. *Journal of Atmospheric Sciences*, 43, 3159–3176. Available from: https://doi.org/10.1175/1520-0469(1986)043<3159:EOTZMS>2.0.CO;2

Hitchman, M.H. & Leovy, C.B. (1988) Estimation of the kelvin wave contribution to the semiannual oscillation. *Journal of Atmospheric Sciences*, 45, 1462–1475. Available from: https://doi.org/10.1175/1520-0469(1988)045<1462:EOTKWC>2.0.CO;2

Holton, J.R. & Tan, H.-C. (1980) The influence of the equatorial quasi-biennial oscillation on the global circulation at 50 mb. *Journal of Atmospheric Sciences*, 37, 2200–2208. Available from: https://doi.org/10.1175/1520-0469(1980)037<2200:TIOTEQ>2.0.CO;2

Holton, J.R. & Wehrbein, W.M. (1980) A numerical model of the zonal mean circulation of the middle atmosphere. *Pure and Applied Geophysics*, 118, 284–306. Available from: https://doi.org/10.1007/BF01586455

Hopkins, R.H. (1975) Evidence of polar-tropical coupling in upper stratospheric zonal wind anomalies. *Journal of Atmospheric Sciences*, 32, 712–719. Available from: https://doi.org/10.1175/1520-0469(1975)032<0712:EOPTCI>2.0.CO;2

Kawatani, Y., Hirooka, T., Hamilton, K., Smith, A.K. & Fujiwara, M. (2020) Representation of the equatorial stratopause semiannual oscillation in global atmospheric reanalyses. *Atmospheric Chemistry and Physics*, 20, 9115–9133. Available from: https://doi.org/10.5194/acp-20-9115-2020

Kidston, J., Scaife, A.A., Hardiman, S.C., Mitchell, D.M., Butchart, N., Baldwin, M.P. et al. (2015) Stratospheric influence on tropospheric jet streams, storm tracks and surface weather. *Nature Geoscience*, 8, 433–440. Available from: https://doi.org/10.1038/ngeo2424

Krismer, T.R., Giorgetta, M.A. & Esch, M. (2013) Seasonal aspects of the quasi-biennial oscillation in the max Planck institute earth system model and ERA-40. *J Adv Model Earth Syst*, 5, 406–421. Available from: https://doi.org/10.1002/jame.20024

Lee, H.-K., Kang, M.-J., Chun, H.-Y., Kim, D. & Shin, D.-B. (2022) Characteristics of latent heating rate from GPM and convective gravity wave momentum flux calculated using the GPM data. *Journal of Geophysical Research: Atmospheres*, 127, e2022JD037003. Available from: https://doi.org/10.1029/2022JD037003

Lieberman, R.S., France, J., Ortland, D.A. & Eckermann, S.D. (2021) The role of inertial instability in cross-hemispheric coupling. *Journal of the Atmospheric Sciences*, 78, 1113–1127. Available from: https://doi.org/10.1175/JAS-D-20-0119.1

Liu, C., Alexander, J., Richter, J. & Bacmeister, J. (2022) Using TRMM latent heat as a source to estimate convection induced gravity wave momentum flux in the lower stratosphere. *Journal of Geophysical Research: Atmospheres*, 127, e2021JD035785. Available from: https://doi.org/10.1029/2021JD035785

Lott, F. & Miller, M.J. (1997) A new subgrid-scale orographic drag parametrization: its formulation and testing. *Quarterly Journal of the Royal Meteorological Society*, 123, 101–127. Available from: https://doi.org/10.1002/qj.49712353704

Lu, H., Gray, L.J., Martineau, P., King, J.C. & Bracegirdle, T.J. (2021) Regime behavior in the upper stratosphere as a precursor of stratosphere–troposphere coupling in the Northern Winter. *Journal of Climate*, 34, 7677–7696. Available from: https://doi.org/10.1175/JCLI-D-20-0831.1

Marshall, A.G. & Scaife, A.A. (2009) Impact of the QBO on surface winter climate. *Journal of Geophysical Research: Atmospheres*, 114, D18110. Available from: https://doi.org/10.1029/2009JD011737

McFarlane, N.A. (1987) The effect of orographically excited gravity wave drag on the general circulation of the lower stratosphere and troposphere. *Journal of Atmospheric Sciences*, 44, 1775–1800. Available from: https://doi.org/10.1175/1520-0469(1987)044<1775:TEOOEG>2.0.CO;2

Meyer, W.D. (1970) A diagnostic numerical study of the semiannual variation of the zonal wind in the tropical stratosphere and mesosphere. *Journal of Atmospheric Sciences*, 27, 820–830. Available from: https://doi.org/10.1175/1520-0469(1970)027<0820:ADNSOT>2.0.CO;2

Molod, A., Takacs, L., Suarez, M. & Bacmeister, J. (2015) Development of the GEOS-5 atmospheric general circulation model: evolution from MERRA to MERRA2. *Geoscientific Model Development*, 8, 1339–1356. Available from: https://doi.org/10.5194/gmd-8-1339-2015

Mukougawa, H., Hirooka, T. & Kuroda, Y. (2009) Influence of stratospheric circulation on the predictability of the tropospheric northern annular mode. *Geophysical Research Letters*, 36, L08814. Available from: https://doi.org/10.1029/2008GL037127

Müller, K.M., Langematz, U. & Pawson, S. (1997) The stratopause semiannual oscillation in the Berlin troposphere–stratosphere–mesosphere GCM. *Journal of the Atmospheric Sciences*, 54, 2749–2759. Available from: https://doi.org/10.1175/1520-0469(1997)054<2749:TSSOIT>2.0.CO;2

Orr, A., Bechtold, P., Scinocca, J., Ern, M. & Janiskova, M. (2010) Improved middle atmosphere climate and forecasts in the ECMWF model through a nonorographic gravity wave drag parameterization. *Journal of Climate*, 23, 5905–5926. Available from: https://doi.org/10.1175/2010JCLI3490.1

Pahlavan, H.A., Fu, Q., Wallace, J.M. & Kiladis, G.N. (2021) Revisiting the quasi-biennial oscillation as seen in ERA5. Part I: description and momentum budget. *Journal of the Atmospheric Sciences*, 78, 673–691. Available from: https://doi.org/10.1175/JAS-D-20-0248.1

Plumb, R.A. (1983) Baroclinic instability of the summer mesosphere: a mechanism for the quasi-two-day wave? *Journal of Atmospheric Sciences*, 40, 262–270. Available from: https://doi.org/10.1175/1520-0469(1983)040<0262:BIOTSM>2.0.CO;2

Polichtchouk, I., Hogan, R., Shepherd, T.G., Bechtold, P., Stockdale, T., Malardel, S. et al. (2017) What influences the middle atmosphere circulation in the IFS? *ECMWF Technical Memoranda*, 809, 1–48. Available from: https://doi.org/10.21957/mfsnfv15o

Quiroz, R.S. & Miller, A. (1967) Note on the semi-annual wind VARIATION in the equatorial stratosphere. *Monthly Weather Review*, 95, 635–641. Available from: https://doi.org/10.1175/1520-0493(1967)095<0635:NOTSAW>2.3.CO;2

Rapp, M., Dörnbrack, A. & Preusse, P. (2018) Large midlatitude stratospheric temperature variability caused by inertial instability: a potential source of bias for gravity wave Climatologies. *Geophysical Research Letters*, 45(10), 610–682. Available from: https://doi.org/10.1029/2018GL079142

Ray, E.A., Alexander, M.J. & Holton, J.R. (1998) An analysis of the structure and forcing of the equatorial semiannual oscillation in zonal wind. *Journal of Geophysical Research: Atmospheres*, 103, 1759–1774. Available from: https://doi.org/10.1029/97JD02679

Reed, R.J. (1966) Zonal wind behavior in the equatorial stratosphere and lower mesosphere. *Journal of Geophysical Research*, 1896-1977(71), 4223–4233. Available from: https://doi.org/10.1029/JZ071i018p04223

Richter, J.H., Sassi, F. & Garcia, R.R. (2010) Toward a physically based gravity wave source parameterization in a general circulation model. *Journal of the Atmospheric Sciences*, 67, 136–156. Available from: https://doi.org/10.1175/2009JAS3112.1

Salby, M.L. (1984) Survey of planetary-scale traveling waves: the state of theory and observations. *Reviews of Geophysics*, 22, 209–236. Available from: https://doi.org/10.1029/RG022i002p00209

Scaife, A.A., Knight, J.R., Vallis, G.K. & Folland, C.K. (2005) A stratospheric influence on the winter NAO and North Atlantic surface climate. *Geophysical Research Letters*, 32, L18715. Available from: https://doi.org/10.1029/2005GL023226

Shepherd, T.G., Polichtchouk, I., Hogan, R. & Simmons, A.J. (2018) Report on stratosphere task force. https://doi.org/10.21957/0vkp0t1xx

Shu, J., Tian, W., Hu, D., Zhang, J., Shang, L., Tian, H. et al. (2013) Effects of the quasi-biennial oscillation and stratospheric semiannual oscillation on tracer transport in the upper stratosphere. *Journal of the Atmospheric Sciences*, 70, 1370–1389. Available from: https://doi.org/10.1175/JAS-D-12-053.1

Smith, A.K., Garcia, R.R., Moss, A.C. & Mitchell, N.J. (2017) The semiannual oscillation of the tropical zonal wind in the middle atmosphere derived from satellite geopotential height retrievals.

Journal of the Atmospheric Sciences, 74, 2413–2425. Available from: https://doi.org/10.1175/JAS-D-17-0067.1

Smith, A.K., Gray, L.J. & Garcia, R.R. (2023) Evidence for the influence of the quasi-biennial oscillation on the semiannual oscillation in the tropical middle atmosphere. *Journal of the Atmospheric Sciences*, 80, 1755–1769. Available from: https://doi.org/10.1175/JAS-D-22-0255.1

Smith, A.K., Holt, L.A., Garcia, R.R., Anstey, J.A., Serva, F., Butchart, N. et al. (2019) The equatorial stratospheric semiannual oscillation and time-mean winds in QBOi models. *Quarterly Journal of the Royal Meteorological Society*, 148, 1593–1609. Available from: https://doi.org/10.1002/qj.3690

SPARC. (2022) SPARC reanalysis intercomparison project (S-RIP) final report. In: Fujiwara, M., Manney, G.L., Gray, L.J. & Wright, J.S. (Eds.) Germany: *SPARC Report No. 10, WCRP-6/2021*. Available from: https://doi.org/10.17874/800dee57d13

Strube, C., Ern, M., Preusse, P. & Riese, M. (2020) Removing spurious inertial instability signals from gravity wave temperature perturbations using spectral filtering methods. *Atmospheric Measurement Techniques*, 13, 4927–4945. Available from: https://doi.org/10.5194/amt-13-4927-2020

Wallace, J.M. (1967) A note on the role of radiation in the biennial oscillation. *Journal of Atmospheric Sciences*, 24, 598–599. Available from: https://doi.org/10.1175/1520-0469(1967)024<0598:ANOTRO>2.0.CO;2

Wallace, J.M. & Holton, J.R. (1968) A diagnostic numerical model of the quasi-biennial oscillation. *Journal of Atmospheric Sciences*, 25, 280–292. Available from: https://doi.org/10.1175/1520-0469(1968)025<0280:ADNMOT>2.0.CO;2

Webb. (1967) In: Webb, W.L. (Ed.) *Structure of the stratosphere and mesosphere*. New York and London: Academic Press, p. 382.

Wheeler, M. & Kiladis, G.N. (1999) Convectively coupled equatorial waves: analysis of clouds and temperature in the wavenumber–frequency domain. *Journal of the Atmospheric Sciences*, 56, 374–399. Available from: https://doi.org/10.1175/1520-0469(1999)056<0374:CCEWAO>2.0.CO;2

SUPPORTING INFORMATION

Additional supporting information can be found online in the Supporting Information section at the end of this article.

How to cite this article: Jaison, A.M., Gray, L.J., Osprey, S., Smith, A.K. & Garcia, R.R. (2024) A momentum budget study of the semi-annual oscillation in the Whole Atmosphere Community Climate Model. *Quarterly Journal of the Royal Meteorological Society*, 1–22. Available from: https://doi.org/10.1002/qj.4782